Airway Gas Exchange and Exhaled Biomarkers

Steven C. George[*1,2] *and Michael P. Hlastala*[3,4]

ABSTRACT

During inspiration and expiration, gases traverse the conducting airways as they are transported between the environment and the alveolar region of the lungs. The term "conducting" airways is used broadly as the airway tree is thought largely to provide a conduit for the respiratory gases, oxygen and carbon dioxide. However, despite a significantly smaller surface area, and thicker barrier separating the gas phase from the blood when compared to the alveolar region, the airway tree can participate in gas exchange under special conditions such as high water solubility, high chemical reactivity, or production of the gas within the airway wall tissue. While these conditions do not apply to the respiratory gases, other gases demonstrate substantial exchange of the airways and are of particular importance to the inflammatory response of the lungs, the medical-legal field, occupational health, metabolic disorders, or protection of the delicate alveolar membrane. Given the significant structural differences between the airways and the alveolar region, the physical determinants that control airway gas exchange are unique and require different models (both experimental and mathematical) to explore. Our improved physiological understanding of airway gas exchange combined with improved analytical methods to detect trace compounds in the exhaled breath provides future opportunities to develop new exhaled biomarkers that are characteristic of pulmonary and systemic conditions. © 2011 American Physiological Society. *Compr Physiol* 1:1837-1859, 2011.

Introduction

The upper respiratory tract and lower airways provide a passage for the transport of the respiratory gases (oxygen and carbon dioxide) between the atmosphere and the alveolar region of the lungs. Hence, the term "conducting" airways is commonly used to describe this portion of the respiratory system. However, the conducting airways can be active participants in the exchange of nonrespiratory gases such as water, ethanol, or nitric oxide (NO) due to significantly different physical characteristics of the gas (e.g., water solubility) or from endogenous production within the airway wall tissue. The exchange of nonrespiratory gases can play important roles in maintaining normal respiratory gas exchange (humidification of inspired air), the medical-legal system (alcohol breath test), occupational health (exposure to volatile solvents such as acetone or formaldehyde), and prominent inflammatory diseases of the lungs such as asthma (exposure to NO). This article will describe the anatomical structure of the upper and lower airways, the physical determinants of gas exchange, models to understand airway gas exchange, several examples of gases that exchange in the airways, and finally how exhaled gases can be used as markers of biological function.

Structure of the Upper and Lower Airway Tracts

The structure of the upper respiratory tract and lower airways strongly influences the function and differs markedly from that of the alveolar region. Both regions participate in airway gas exchange, but their respective structures dictate additional functions as well.

Upper respiratory tract

The upper respiratory tract is normally considered to include the nasal cavity, the oral cavity, the oro- and nasopharynx, and the larynx (Fig. 1). Tidal breathing normally includes inspiration through the nasal cavity (nasal or nose breathing) where the airstream comes into contact with a large surface area contributed by the superior, middle, and inferior nasal conchae ("turbinates"). The conchae not only contribute a large surface area but also induce turbulent mixing of the air (see below), both of which act to serve a primary role in the warming and humidification of the inspired air. Once air passes the nasal cavity, it enters the pharynx, which is divided

[*]Correspondence to scgeorge@uci.edu

[1]Department of Biomedical Engineering, University of California, Irvine, California

[2]Department of Chemical Engineering & Materials Science, University of California, Irvine, California

[3]Department of Physiology and Biophysics, University of Washington, Seattle, Washington

[4]Department of Medicine, University of Washington, Seattle, Washington

Published online, October 2011 (comprehensivephysiology.com)

DOI: 10.1002/cphy.c090013

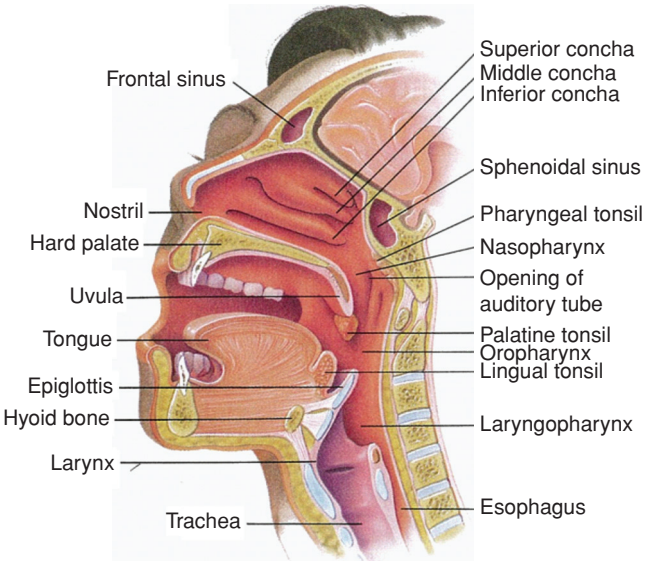

Figure 1 Major anatomical features of the upper respiratory tract. Gross anatomical structures in the upper respiratory tract including the nasal cavity, conchae, teeth, tongue, uvula, oropharynx, nasopharynx, and larynx. From reference 136.

into three regions (Fig. 1): the nasopharynx, the oropharynx, and the laryngopharynx. The latter is bordered superiorly by the posterior surface of the epiglottis. During oral or mouth breathing, the airstream enters the oral cavity, where, similar to the nasal cavity, it encounters significant anatomical structures including the teeth, tongue, and uvula (Fig. 1), which can induce turbulent mixing and/or enhance the surface area for warming and humidification of the airstream. Air exits the oral cavity and enters the oropharynx (continuous with the nasopharynx), before passing through the laryngopharynx and larynx (Fig. 2A). The larynx contains the vocal cords and thus has a dynamic internal diameter that can create significant turbulent mixing of the airstream.

The entire upper respiratory tract is lined by a thin mucous membrane that serves a primary role in the humidification of the inspired air. Beneath the mucous layer is the epithelium whose structure depends on the anatomical region. The oral cavity and the oropharynx contain a nonkeratinized squamous (flat, multicell layered) epithelium, whereas the nasal cavity epithelium is pseudostratified, cilated, and columnar (tall, single-cell layer). The epithelium of the larynx is mixed, containing both nonkeratinized, squamous and pseudostratified, cilated, columnar epithelia. The structure of the epithelium can potentially influence airway gas exchange, as it represents a physical and metabolic barrier separating the airstream from the circulation.

The epithelium rests on the basement membrane, a thin layer of collagen, which separates the epithelium from the lamina propria. The lamina propria is a layer of connective tissue that contains mucous and serous glands, as well as a blood supply. The rate of blood flow and the distance separating the blood from the airstream can influence airway gas exchange (see below).

Lower respiratory tract

The lower respiratory tract includes all anatomical structures below the larynx, beginning with the trachea and ending with the alveoli. The trachea divides at the carina into the left and right main stem bronchi, which further divide into the lobar bronchi. Each branch generally gives rise to two daughter branches and thus beginning at the trachea (generation 0), the airway tree can be described as a bifurcating tree structure where each bifurcation gives rise to the next airway generation (Figs. 2A and 2B). The average physical dimensions (length and diameter) of the airway tree for a typical adult human are described in Weibel's classic text (169), and the summary for an idealized symmetric bifurcating tree ("model A") is shown in Table 1. Note that each daughter branch is shorter in length and smaller in diameter. The length:diameter ratio for each generation is nearly constant at ~3, and the ratio of the diameter of the parent to the daughter branches is also nearly constant at ~1.2. It can be easily shown that this design ensures that the resistance to laminar flow [see Eq. (3) below] through the daughter branches (two tubes in parallel) is approximately equal to the parent branch.

Several important physical characteristics of the airway tree relevant to gas exchange are the volume (V_{aw}) and surface area (A_{aw}), both of which scale with the size of the individual. For children, V_{aw} (ml) is proportional to height and can be approximated by $V_{aw} = 1.018 \times \text{Height (cm)} - 76.2$ (74). For adults, a convenient means of estimating V_{aw} (ml) is to simply add the ideal body weight (lb) of subjects plus their age in years (21,170). Thus, for a 40-year-old adult whose ideal body weight is 160 lb, an estimate of V_{aw} is 200 ml. Correlations between body size (e.g., height or weight) and the surface area are not commonly used but are easily calculated, given V_{aw} and a symmetric bifurcating structure. In the example given above, A_{aw} would be 8900 cm^2.

Characteristics of the epithelium progressively change as airway generation increases, reflecting the primary function of the larger airways compared with the smaller airways. The epithelium in the trachea is pseudostratified, cilated, and columnar, with numerous goblet cells (mucous producing) and a thickness of approximately 100 μm (Fig. 2C). As airway generation increases, the thickness of the epithelium decreases (approximately 20 μm by generation 12-15), as well as the density of cilia and goblet cells, reflecting the transition to the respiratory gas exchange region of the alveoli characterized by a very thin squamous epithelium lined by surfactant. The presence of cilia in the upper airways serves to trap inhaled particles and transport them proximally in the mucous layer where the debris can be removed in the digestive tract. While difficult to characterize *in vivo*, the mucous layer is approximately 10 μm thick (94). Similar to the pharynx, the epithelium rests on a thin basement membrane that

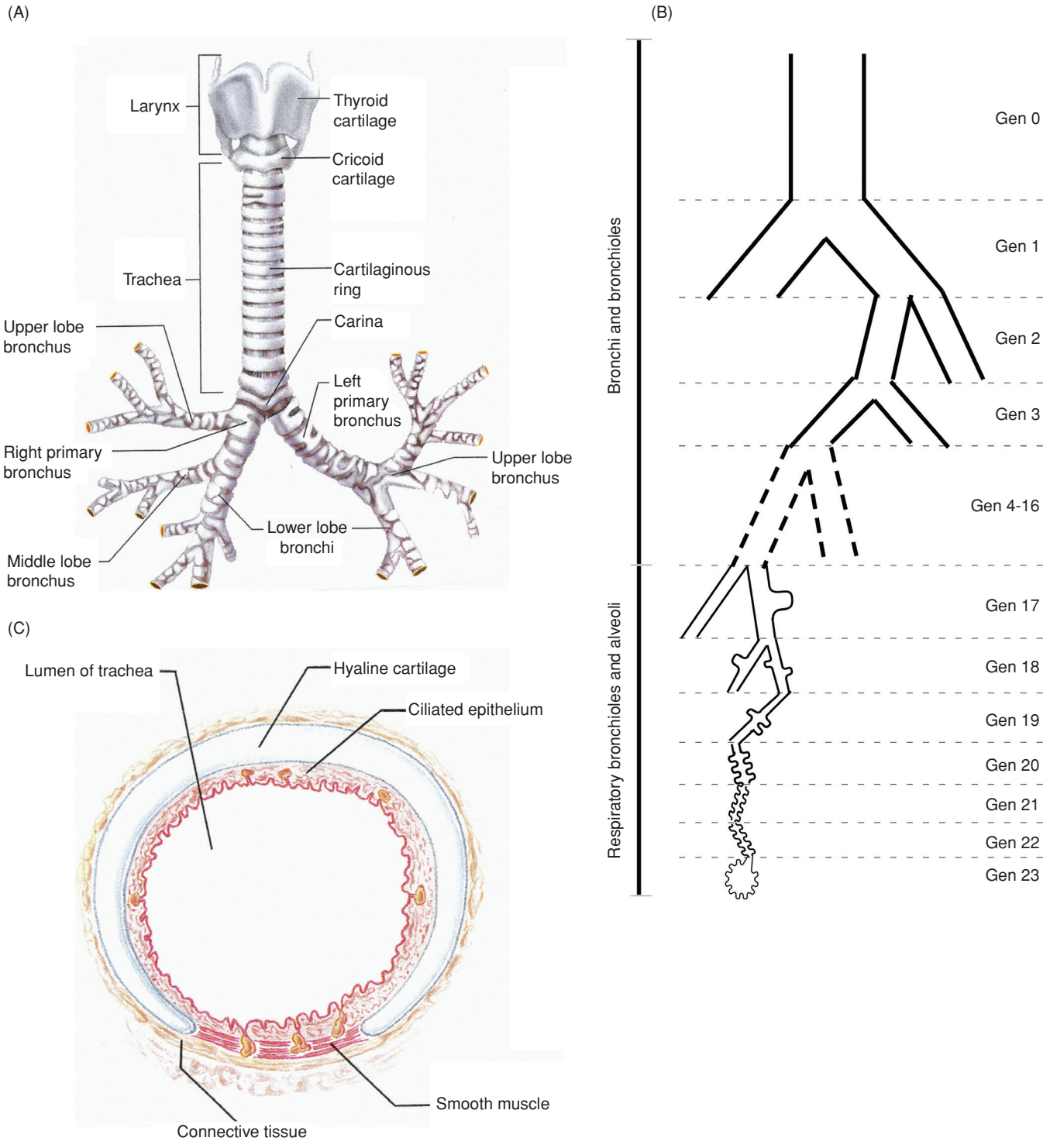

Figure 2 Major anatomical features of the lower respiratory Tract. (**A**) Schematic of the gross anatomical features of the branching structure of the airway tree, and identifying trachea, main stem bronchi, and major lobar bronchi. (**B**) Schematic mapping the airways to generation number from the trachea (generation 0) to the respiratory bronchioles and alveoli (generations 17-23). (**C**) Cross-section of trachea at higher magnification demonstrating the layer of the airway wall including the epithelium, cartilage ring, and subepithelial connective tissue. From reference 136.

Table 1

Generation	Diameter (cm)	Length (cm)	Cross-sectional area (cm^2)	Cumulative cross-sectional area (cm^2)	Surface area (cm^2)	Cumulative surface area (cm^2)	Volume (cm^3)	Cumulative volume (cm^3)
0	1.8	12	2.54	2.54	67.8	67.8	30.5	30.5
1	1.22	4.8	2.34	4.9	36.8	105	11.2	41.8
2	0.83	1.9	2.16	7.0	19.8	124	4.11	45.9
3	0.56	0.8	1.97	9.0	11.3	136	1.58	47.4
4	0.45	1.3	2.54	11.6	29.4	165	3.31	50.8
5	0.35	1.1	3.08	14.6	38.7	204	3.39	54.1
6	0.28	0.9	3.94	18.6	50.6	254	3.55	57.7
7	0.23	0.76	5.32	23.9	70.3	325	4.04	61.7
8	0.19	0.64	7.26	31.2	97.7	422	4.65	66.4
9	0.15	0.54	9.05	40.2	130	553	4.89	71.3
10	0.13	0.46	13.6	53.8	192	745	6.25	77.5
11	0.11	0.39	19.5	73.3	276	1,020	7.59	85.1
12	0.095	0.33	29.0	102	403	1,420	9.58	94.7
13	0.082	0.27	43.3	146	570	1,990	11.7	106
14	0.074	0.23	70.5	216	876	2,870	16.2	123
15	0.066	0.2	112	328	1,360	4,230	22.4	145
16	0.06	0.16	185	513	1,980	6,210	29.6	175
17	0.054	0.14	300	814	3,100	9,320	42.0	217
18	0.05	0.12	515	1,330	4,940	14,300	61.8	278
19	0.047	0.099	910	2,240	7,660	22,000	90.1	370
20	0.045	0.083	1,670	3,910	12,300	34,300	139	510
21	0.043	0.07	3,050	6,960	19,800	54,100	214	720
22	0.041	0.059	5,540	12,500	32,900	86,000	327	1,050
23	0.041	0.05	54,000	66,500	54,000	140,000	2,700	3,750

separates the epithelium from the lamina propria and the bronchial circulation.

Physical Phenomena Governing Airway Gas Exchange

Gas exchange implies the net transport of a gas from one location to another and is thus governed by the mechanisms of transport (convection and diffusion), as well as other physical and chemical phenomena including solubility (in water or tissue), vapor-liquid equilibrium, and chemical reaction.

Convection and diffusion

There are two major mechanisms that can create a net transport of gas—convection and molecular diffusion. Convection is transport due to the bulk movement of fluid, whereas molecular diffusion is transport due to motion of particles from their internal energy. If a gas is present in a flowing fluid, the bulk movement of the fluid leads to transport of the gas in the direction and rate of the moving fluid. If spatial density gradients are the cause of the bulk fluid movement, the process is known as *free convection*. In contrast, if an external hydrostatic pressure difference causes the bulk flow, the process is referred to as *forced convection* (i.e., advection). For gas exchange in the airways, free convection is generally negligible and the bulk movement of air through the airways during inspiration or expiration is by forced convection, caused by the hydrostatic pressure difference relative to ambient pressure created by the respiratory muscles, and the elastic recoil of the chest wall and lungs. Over the time, scales of interest for airway gas exchange (order seconds), convection is an important mechanism of transport over length scales of the order of millimeters to meters and can be characterized quantitatively by simply the velocity, v (cm/s), of the bulk fluid in the direction of interest.

Convective flow of a fluid can be either laminar or turbulent. In laminar flow, the movements of all fluid "elements" are in the direction of the bulk flow, and the velocity depends on the position of the fluid element. For example, the airways are generally considered rigid tubes in which the fluid adjacent to the tube wall has a zero velocity ("no-slip" condition). A momentum balance over a differential volume element in the fluid produces a parabolic velocity profile (18) in which the velocity in the z-direction depends on the radial position squared (Fig. 3A):

$$v(r) = \frac{(\Delta P)R^2}{4\mu L}\left[1 - \left(\frac{r}{R}\right)^2\right] \quad (1)$$

where L is the tube length (cm), μ is fluid viscosity, and the external pressure difference across the length of the tube is ΔP. The average velocity, $<v>$, is simply calculated by integrating all of the velocities over the cross-sectional area

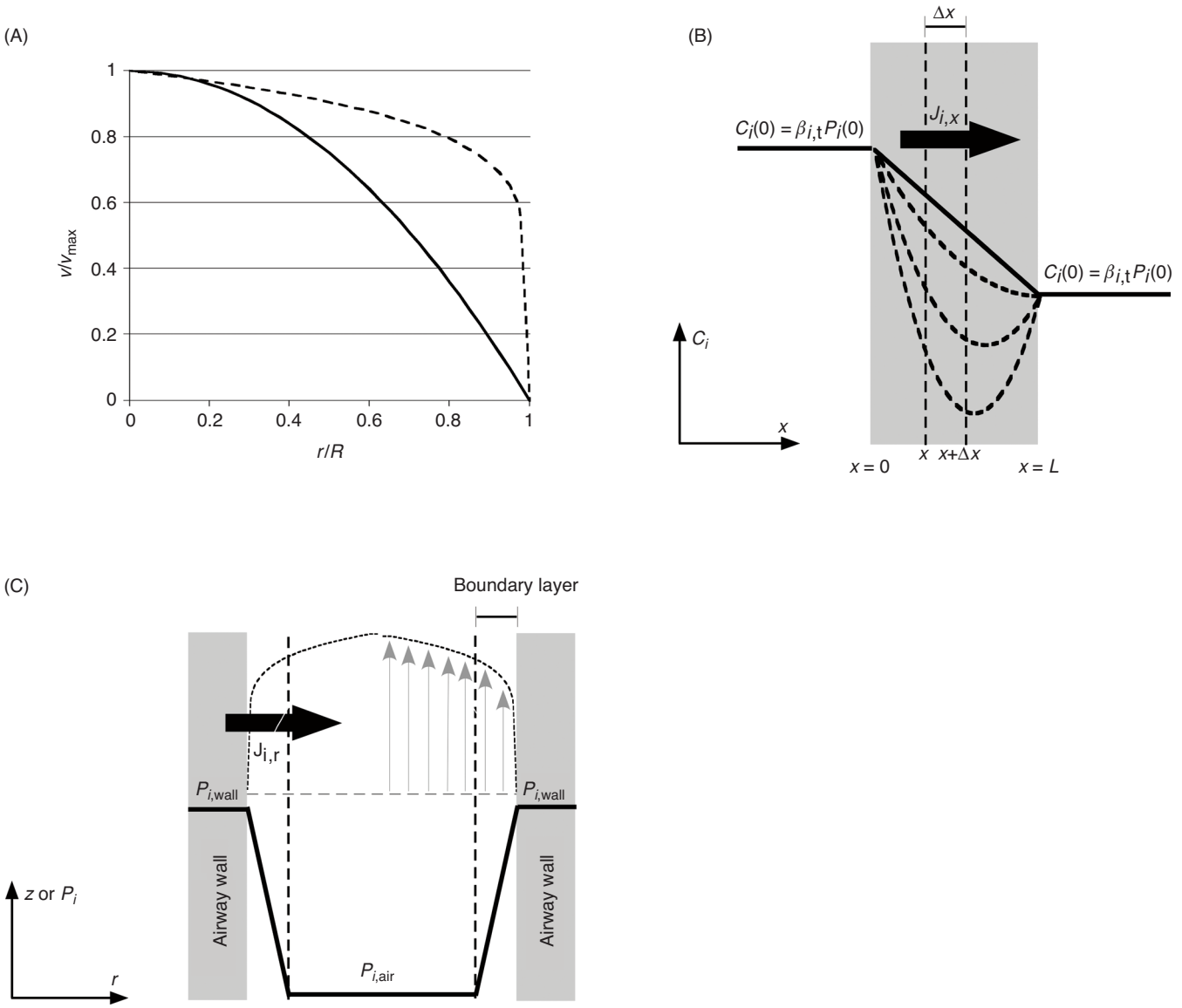

Figure 3 Convection and diffusion in the airways. (**A**) laminar (solid line) and turbulent (dashed line) flow velocity distributions within a cylinder or tube. The velocity, v, is normalized by the maximum velocity, v_{max} (at the centerline), and is plotted as a function of radial position, r, normalized by the radius of the tube, R. The laminar and turbulent flow profiles are described in the text [Eqs. (1) and 4]. (**B**) schematic of the steady-state concentration profile of a gas across a thin membrane (e.g., the airway wall) of thickness L. The solid line depicts an unreactive gas, while the dashed lines depict progressively more reactive gases that are consumed within the membrane. Symbols are described in the text. (**C**) Schematic of a turbulent flow profile within a sagittal section of a tube and the corresponding partial pressure profile (solid line) across the tube. The pressure of the gas drops rapidly across the boundary layer and then is constant due to turbulent mixing. The resistance to mass transfer is from the boundary layer and can be characterized by a mass transfer coefficient. Additional details and definition of symbols are provided in the text.

and then dividing by the cross-sectional area (18):

$$< v > = \frac{\Delta(P)R^2}{8\mu L} \qquad (2)$$

Finally, the well-known relationship in which the average volumetric flow, $< \dot{V} >$, is proportional to the tube radius raised to the fourth power (Hagen-Poiseuille law) is determined by simply multiplying $< v >$ by the cross-sectional area:

$$< \dot{V} >= \frac{(\Delta P)\pi R^4}{8\mu L} \qquad (3)$$

It can also be seen from Eq. (3) that the resistance to flow through a tube for laminar flow is $8\mu L/\pi R^4$. Laminar flow is sometimes referred to as "low" or "small" flows. As the flow increases, it becomes turbulent. Turbulent flow is characterized by fluid elements moving randomly (and thus in all directions), while the bulk fluid is characterized by the

movement in a single direction. While a precise solution of the velocity distributions is not possible, a practical approach is to use the time-averaged velocity at a given radial position, v, which has been described mathematically as

$$v(r) = v_{max}\left[1 - \left(\frac{r}{R}\right)^{1/7}\right] \quad (4)$$

for turbulent flow in tubes where v_{max} is the maximum velocity at the centerline (Fig. 3A). The transition from laminar to turbulent flow depends on many factors, such as surface roughness, but in smooth tubes it occurs at approximately a Reynolds number (Re) of 2100, where $Re = D<v>\rho\mu$ (D = tube diameter). For 2100 < Re < 100,000, the average volumetric flow is given by

$$< \dot{V} >= K(\Delta P)^{7/4} \quad (5)$$

where K is simply a coefficient of proportionality that depends on fluid viscosity and the physical dimensions of the tube. Note the stronger dependence of $< \dot{V} >$ on the pressure drop in turbulent flow than that in laminar flow.

The second mechanism that can create a net transport of a gas is molecular diffusion. As the name implies, molecular diffusion occurs due to the internal energy (e.g., vibrational) of individual molecules resulting in Brownian motion. While Brownian motion is the random movement of a molecule, net transport of a gas can occur if a spatial concentration gradient of the gas exists. In this case, net transport occurs from a position of high concentration to a position of lower concentration, or in the opposite direction of the concentration gradient. Fick's first law of diffusion is an empirical description that quantitatively describes the rate of transport due to diffusion and

$$J_i i = -D_{i,B}\nabla C_i \quad (6)$$

where J_i is the flux of gas (ml of gas STPD s^{-1} cm^{-2}) in three dimensions, $D_{i,B}$ is the molecular diffusivity of gas i in medium B (e.g., air, cm^2/s), C_i is the concentration (ml of gas STPD cm^{-3} medium) of gas i, and ∇ is the gradient operator vector in three dimensions. The concentration of a gas is proportional to the partial pressure and solubility and is described in detail in the next section. Note that Eq. (6) easily reduces to one dimension. For example, in cylindrical coordinates, if diffusion of a gas occurs only in the radial direction, r, then ∇ reduces to d/dr. Fick's first law of diffusion is valid for dilute (concentration of gas i in medium B < 5 mole%) solutions and hence for most physiological conditions.

Over the time scales of interest for airway gas exchange (order seconds), diffusion is an important mechanism of transport over length scales of the order of microns to millimeters and can be characterized quantitatively by a characteristic velocity of diffusion, υ_{diff} (cm/s), in the opposite direction of the concentration gradient,

$$v_{diff} = \frac{D_{i,B}}{L_{diff}} \quad (7)$$

where L_{diff} is a characteristic length of diffusion for the geometry of interest (e.g., radius of tube for radial diffusion in cylindrical coordinates). In many applications, it is convenient to consider the relative magnitude of convection to diffusion. This is classically accomplished using the Peclet number (Pe), which is the ratio of the velocity of convection of mass to the velocity of diffusion of mass. For flow in a tube of radius R,

$$Pe = \frac{<Q>}{RD_{i,B}} \quad (8)$$

where L_{diff} has been replaced with the radius of the tube. The Pe is a convenient nondimensional number that can be used to quickly assess the relative importance of convection and diffusion on the rate of transport. For airway gas exchange, this is particularly useful when creating mathematical models. For example, when the Pe is large (>10), diffusion can be neglected in the mathematical formulations, allowing for a more tractable quantitative description.

Water solubility and vapor-liquid equilibrium

A gas can be transported by a fluid only if it is soluble in that fluid; that is, when a gas is placed in contact with a liquid, a fraction of the gas dissolves into the liquid. Since most tissue and blood are predominantly water, the solubility of a gas in water is a useful approximation to describe gas exchange. Consider a simple example where a gas i, with a partial pressure P_i (mmHg), is placed in a closed container with a liquid and allowed to come to equilibrium. If the gas is soluble in the liquid, then a concentration, C_i (or mole fraction, x_i, moles of gas/total moles of liquid), of the gas will be measurable in the liquid. For many gases and liquids, particularly for dilute solutions, the relationship between P_i and C_i is linear; that is, as the partial pressure of the gas increases, the concentration of the gas in the liquid increases proportionally, or,

$$P_i = H_{i,B}x_i \quad (9)$$

where $H_{i,B}$ is Henry's law constant for gas i in liquid medium B and simply represents the coefficient of proportionality. Qualitatively, as the solubility of a gas increases, the concentration of the gas in the liquid will increase; hence, the solubility is the inverse of $H_{i,B}$, and normally denoted as $\beta_{i,B}$. The quantitative description of solubility has a long history, and several excellent textbooks devote significant attention to the topic (124). In physiology, the most commonly encountered units for pressure and concentration are mmHg and ml gas per unit volume of medium; hence, Eq. (9) can be rewritten

slightly,

$$\beta_{i,\mathrm{B}} P_i = C_{i,\mathrm{B}} \tag{10}$$

where the units of $\beta_{i,\mathrm{B}}$ are (ml of gas STPD)(cm^3 medium B)$^{-1}$ mmHg^{-1}, which represents a more frequently encountered form in the physiological literature. Finally, the solubility of a gas in the gas phase itself, $\beta_{i,\mathrm{g}}$, can be expressed using the ideal gas law,

$$\beta_{i,\mathrm{g}} P_i = C_{i,\mathrm{g}} = \frac{V_i}{V} = \frac{P_i}{P} \rightarrow \beta_{i,\mathrm{g}} = \frac{1}{P} \tag{11}$$

where $C_{i,\mathrm{g}}$ is expressed in units ml of gas *i*/ml of gas. It is then common to express the solubility of gas in medium B as the ratio $\beta_{i,\mathrm{B}}/\beta_{i,\mathrm{g}}$, which is known as the Ostwald partition coefficient, $\lambda_{\mathrm{B},i}$, and has the units (ml of gas *i* STPD) (cm^3 medium B)$^{-1}$.

The solubility of a gas in a liquid or liquid-like medium such as tissue depends strongly on temperature. As temperature increases, the solubility of the gas in the liquid decreases. Although body temperature is tightly controlled at 37°C, significant cooling and warming of the airways can occur because of the heat of vaporization of water. The evaporation of water during inspiration to humidify the airstream and the condensation of water during exhalation occur simultaneously with the exchange of other gases, so the surface of the airways can cool and warm, respectively. Detailed models of this phenomenon have been presented (160, 161) and suggest that even during normal quiet tidal breathing, the temperature of the tracheal wall can decrease to 30°C. This change in temperature can significantly alter gas solubility.

The regions used for gas exchange depends strongly on the both the blood solubility (λ_{b}) and the water solubility (λ_{w}) of the gas. Generally, gases of lower blood solubility ($\lambda_{\mathrm{b}} < 1$) exchange predominantly in the alveoli with the pulmonary circulation and gases of higher blood solubility ($\lambda_{\mathrm{b}} > 500$) exchange predominantly in the airways with the bronchial circulation. A mathematical model was used to predict this distribution of gas exchange (4). Figure 4 shows relative airway gas exchange normalized by the total (airway and alveolar) gas exchange. Low-solubility inert gases such as sulfur hexafluoride, ethane, and cyclopropane exchange entirely in the alveoli, whereas high-solubility gases such as isopropanol, ethanol, and methanol exchange entirely in the airways. The gases of intermediate solubility ($1 < \lambda_{\mathrm{b}} < 500$), such as isoflurane, halothane, diethyl ether, methyl ethyl ketone, and acetone, exchange partially in the alveoli and partially in the airways. It is important to remember that the balance of airway and alveolar gas exchange is symmetric, whether the gas is being absorbed or eliminated. For highly soluble gases absorbed or eliminated through the airways, the process is also dependent on λ_{w} relative to λ_{b} because of airway tissue water (5).

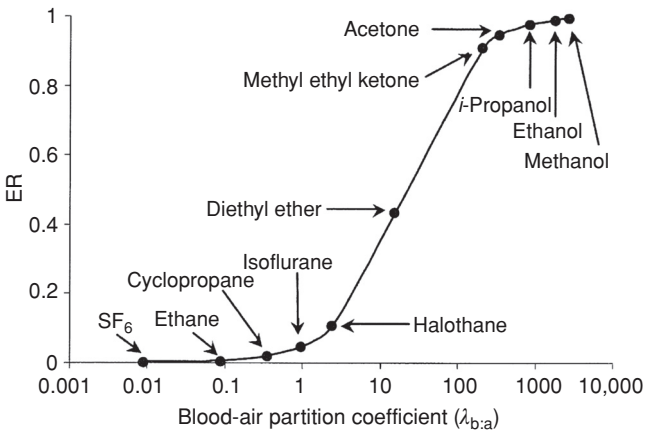

Figure 4 The exchange ratio (ER) is the ratio of airway gas exchange to the total of airway and alveolar gas exchange. Low-solubility gases exchange in the alveoli while high-solubility gases exchange in the airways. Intermediate solubility gases exchange in both the airways and the alveoli. From reference 4.

Energy and mass transfer

The transfer of mass (i.e., gases) and energy (i.e, heat) between the airstream and airway wall during respiration can be quantitatively described using the same approach as the transfer of energy and mass between a solid surface and a flowing fluid. Both diffusion and convection influence the rate of transfer. Diffusion is the mechanism by which either energy or mass is transported across the surface-fluid interface because of either a concentration or temperature difference between the surface and the fluid; however, the presence of flow enhances the gradient and hence the rate of transfer. As an example, consider the steady-state transport of a gas (gas "i") across a thin piece of tissue (Fig. 3B), where the partial pressure of the gas on each side is held constant. If the gas is soluble in the membrane, a net flux of gas *i* in the *x*-direction, $J_{i,x}$ (ml of gas STPD cm^{-2} s^{-1}), due to diffusion across the tissue, will commence. The flux at any point in the membrane can be described by Fick's first law of diffusion; hence, for steady-state conditions, the rate of mass entering a differential volume (surface area multiplied by thickness) must equal the rate of leaving, or

$$A D_{\mathrm{i,t}} \frac{\mathrm{d}C_i}{\mathrm{d}x}(x) = A D_{i,\mathrm{t}} \frac{\mathrm{d}C_i}{\mathrm{d}x}(x + \Delta x) \tag{12}$$

where A is the surface area, and $D_{i,\mathrm{t}}$, is the diffusivity of gas i in tissue (subscript t). If A and $D_{i,\mathrm{t}}$ are constant and do not depend on position, then one can divide both sides by $AD_{i,\mathrm{t}}\Delta x$ and take the limit as $\Delta x \rightarrow 0$ to derive a simple second-order differential expression describing how the concentration of the gas depends on the position within the membrane ($\mathrm{d}^2C_i/\mathrm{d}x^2 = 0$). Solving the equation, using the two boundary conditions [e.g., at $x = 0$, $C_i = C_i(0) = \beta_{i,\mathrm{t}} P_i(0)$],

results in the following linear expression for $C_i(x)$:

$$C_i(x) = \frac{\beta_{i,t} x}{L} [P_i(L) - P_i(0)] - C_i(0) \quad (13)$$

where L is the thickness of the membrane, and $\beta_{i,t}$ is the solubility of gas i in tissue (subscript t). Using Fick's first law of diffusion [Eq. (6)] in one dimension, the following expression for the flux of gas across the membrane results:

$$J_{i,x} = -\frac{\beta_{i,t} D_{i,t}}{L} [P_i(L) - P_i(0)] \quad (14)$$

If one multiplies both sides of Eq. (13) by the surface area, then the total rate of transport of gas i in the x-direction, $V_{i,x}$ (ml STPD s^{-1}), is given by,

$$V_{i,x} = -\frac{D_{i,t} A \beta_{i,t}}{L} [P_i(L) - P_i(0)] = D_{i,t} [P_i(0) - P_i(L)] \quad (15)$$

where $D_{i,x}$ is the diffusing capacity (or conductance) of the tissue to gas i in the x-direction and is the product of four constants: the solubility, the surface area, the molecular diffusivity, and the inverse of the membrane thickness. The "driving force" for mass transfer is the partial pressure difference across the tissue. This analysis provides insight into the physical phenomena that can influence the rate of gas transport across a membrane.

Gas exchange from the surface of the airway wall to the flowing gas stream can be described using an analogous approach for steady-state diffusion across a membrane (Fig. 3C). If the gas phase concentration is characterized by a partial pressure at any position z along the airway, and the surface of the airway wall is also characterized by a partial pressure, then by analogy to Eq. (15), as well as the relationship between concentration and partial pressure from Eq. (10), one can describe the steady-state rate of mass transfer (flux, ml of gas STPD s^{-1} cm^{-2}) in the radial direction by,

$$J_{i,r} = k_{i,t} \left[P_{i,wall} - P_{i,air} \right] \quad (16)$$

where $P_{i,air}$ is the partial pressure of gas i in air (mmHg), and $k_{i,t}$ is the convective mass transfer coefficient (ml gas of i cm^{-2} $mmHg^{-1}$) for gas i from a tissue surface. $k_{i,t}$ is analogous to a conductance for mass transfer between the surface and the gas phase per unit surface area (e.g., diffusing capacity divided by the surface area) and thus should also depend on the solubility (in air), molecular diffusivity (in air), and a thickness of the barrier to diffusion. The latter is really an effective thickness of air adjacent to the airway wall that provides the bulk of the resistance to radial diffusion, is generally referred to as the "boundary layer," and most easily understood when flow is turbulent. Recall Eq. (4) that describes the velocity profile for turbulent flow in a tube (Fig. 3A). The thickness of the boundary layer depends on the flow and physical properties of the fluid. As the volumetric flow (or average velocity) increases, the boundary layer becomes thinner because of enhanced turbulent mixing. The smaller boundary layer reduces the resistance to radial mass transfer analogous to a thinner membrane [Eq. (14)]. Hence, the convective mass transfer coefficient for a tube (e.g., an airway) describes the radial mass transfer by diffusion, but its magnitude depends on the rate of axial convection.

Exercise or other activity that increases the volumetric flow of air through the airways will enhance radial heat and mass transfer by not only impacting the concentration in the gas phase but also by reducing the boundary layer resistance. Detailed theoretical and experimental correlations relating the convective mass transfer coefficient to the flow and physical properties for different geometries including tubes can be found in numerous published references (18, 117). In addition, experimental heat and mass transfer coefficients for the unusual geometries of the nasal cavity, oral cavity, and pharynx have been described (54), as well as theoretical estimates for endogenously produced gases in the airways (29).

Chemical reaction

Chemical reaction can clearly impact the rate of mass (and energy) transfer between the airway wall and airstream. Obviously, for a gas to be transferred across the airway wall, there must be a source to generate an airway wall or airstream concentration. This source can be the inhaled air, or it could be the airway wall tissue. For the latter case, the gas may be transported to the airway wall through the bronchial blood, or it may be generated by the cells of the airway wall (e.g., airway epithelial cell). If the airway wall itself produces the gas, it does so through a chemical reaction. Similarly, the gas transported to the airway wall through the blood or produced by the airway wall cells may be consumed by chemical reaction, thus impacting not only the absolute concentration but also the gradient in the concentration. The impact of the latter on the rate of mass transfer between the airway wall and gas stream is less intuitive.

Consider again the example of a gas that is transported across a thin membrane, but in this case the gas is consumed by chemical reaction within the membrane. An example of such a gas is ozone (see below). If the concentration of the gas is held constant at the boundaries of the membrane, then at any position within the membrane, the concentration will be lower than the case with no chemical reaction (dashed line in Fig. 3B). The concentration gradient, and hence the rate of diffusion, is therefore impacted. It should also be apparent that the concentration gradient is not constant and thus the rate of mass transfer in the x-direction depends on the x-position. To illustrate this concept quantitatively, consider the rate of consumption due to chemical reaction to be a constant rate per unit volume for gas i, S_i (ml of gas i cm^{-3}). Then, the mass entering the control volume by diffusion must be equal to the mass leaving by diffusion plus the amount consumed

by chemical reaction or,

$$AD_{i,t}\frac{dC_i}{dx}(x) = AD_{i,t}\frac{dC_i}{dx}(x+\Delta x) + S_i A\Delta x \qquad (17)$$

One can then proceed with the same mathematical steps as described above for the case with no chemical reaction (divide both sides by $AD_{i,t}\Delta x$ and take the limit as $\Delta x \to 0$) to derive an inhomogeneous second-order differential expression describing how the concentration of the gas depends on position within the membrane ($d^2C_i/dx^2 = S_i/D_{i,t}$). The differential expression can again be easily solved by integrating twice, which produces a quadratic equation for $C_i(x)$,

$$C_i(x) = \frac{S_i}{2D_{i,t}}(x^2 - xL) + \frac{\beta_{i,t}}{L}[P_i(L) - P_i(0)] + C_i(0) \qquad (18)$$

Note that Eq. (18) reduces to the case with no chemical reaction [Eq. (12)] for $S_i = 0$. Also, one can then use Fick's first law of diffusion to calculate the rate of mass transfer across each surface, or

$$@x = 0: \quad J_i = \frac{\beta_{i,t}D_{i,t}}{L}[P_i(0) - P_i(L)] + S_i\frac{L}{2} \qquad (19)$$

$$@x = L: \quad J_{i,x} = \frac{\beta_{i,t}D_{i,t}}{L}[P_i(0) - P_i(L)] + S_i\frac{L}{2} \qquad (20)$$

Hence, the impact of chemical reaction can be seen from the second term on the right-hand side of Eqs. (19) and (20). At the surface $x = 0$, chemical reaction enhances the rate of mass transfer by increasing the gradient in concentration, but at the surface $x = L$, the rate of mass transfer is decreased as the gradient in concentration is reduced. Note that if S_i is large enough such that the second term on the right-hand side exceeds the first term, then the flux in the x-direction becomes negative or changes direction. In this case, gas is transported from both boundaries into the thin film. The different cases can be seen graphically in Figure 3B.

Models of Airway Gas Exchange

Models of airway gas exchange can be divided into mathematical and experimental. Mathematical models represent a quantitative or theoretical framework from which to enhance understanding of airway gas exchange principles and are normally used either to generate new hypotheses or to simulate experimental observations. Experimental models represent a physical or biological representation of one or more aspects of airway gas exchange and include inanimate structures, cell cultures, tissue cultures, *ex vivo* animal tissues, *in situ* animal models, and human subjects. The experimental model is designed to understand a specific feature of airway gas exchange to address a hypothesis. Mathematical and experimental models work together to improve our understanding of pulmonary gas exchange.

Mathematical

Mathematical models of airway gas exchange can include descriptions at the cellular level, a single airway, or the entire airway tree. For gas exchange in the airways, few models exist at the cellular level. One example is the microscopic model of NO gas exchange by Shin and George (139). This model describes the production, transport by diffusion, and simultaneous chemical reaction of NO with numerous substrates, in particular *S*-nitrosoglutathione (GSNO), within the confines of the airway epithelium. The model is composed of a set of ordinary differential equations that are solved simultaneously for the steady-state condition.

Mathematical descriptions of flow and gas mixing in single tubes or a single bifurcation have been presented and include both exact analytical solutions and approximate solutions of the momentum (e.g., Navier-Stokes equations for a Newtonian fluid) and mass conservation equations. These models began with fundamental descriptions of flow patterns within a branched network of symmetric bifurcating tubes (133, 134) and then progressed with theoretical descriptions for how the flow patterns would impact longitudinal transport (10, 34, 163), as well as absorption by the airway wall (34, 51). More recent mathematical models have included the impact of flexible, curved, and tapered tubes, oscillatory flow, and small *Pe* number (36, 40, 41, 52).

A detailed anatomical description of the airway tree was first described by Weibel (169), who organized the branching structure into generations where generation 0 represented the trachea, generation 1 the main stem bronchi, and so forth. The human airway tree was described by 23 generations, and detailed dimensions (i.e., lengths and diameters) were provided (Table 1). Generations 1 to 16 represent the bronchi and bronchioles, and generations 17 to 23 represent the respiratory airways where each subsequent generation contained a larger fraction of alveoli. Figure 5 presents the total cross-sectional area of the Weibel symmetric airway tree (model "A") as a function of cumulative distance into the airway tree ($z = 0$ represents the start of the trachea). A simple model of the airway tree is thus a single cylinder with a progressively increasing cross-sectional area reminiscent of the shape of a trumpet; hence, this model is commonly referred to as the single-path trumpet. The cross-sectional area can be described by a power law (exponent of −2.0; dashed line of Fig. 5):

$$A(z) = A_{17}\left(\frac{z}{z_{17}}\right)^{-2} \qquad (21)$$

where z_{17} is the length position at the start of the trumpet (start of generation 17) and A_{17} is the cross-sectional at z_{17}. The simplicity of the single-path trumpet is the most attractive feature and has been used successfully to understand

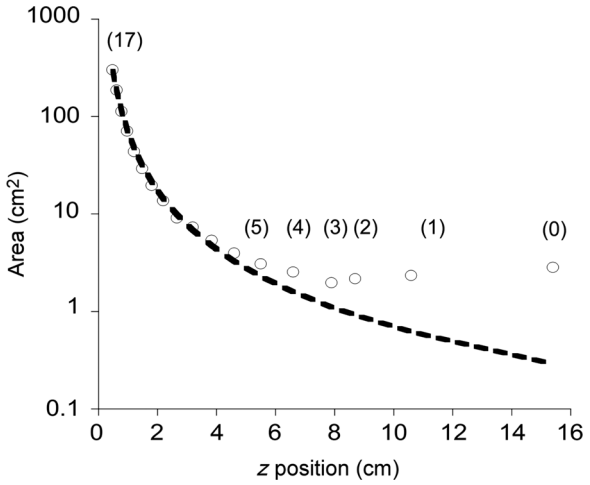

Figure 5 Cross-sectional area of the airway tree. Cross-sectional area (log scale) is shown as a function of axial position within the airway tree. The open circles represent experimental data from Weibel (169), and the dashed line represents an exponential fit: $A(z)=A_{17}(z/z_{17})^{-2}$ [Eq. (21)]. The exponential equation is a good fit between approximately airway generations 5 to 17. The numbers in parentheses represent the airway generation number. The cross-sectional area as a function of length represents the "trumpet" model of the airway tree.

numerous features of airway gas exchange including gas mixing and mass transfer between the surface of the airways and the gas stream (10, 112, 174, 175). In many cases (e.g., steady state), an analytical solution can be achieved (30, 131, 157), which greatly facilities the portability and interpretation of the model.

While serial or longitudinal features of airway gas exchange can be modeled using the single-path trumpet, alternate models are necessary to simulate parallel heterogeneities in ventilation or gas mixing within the large and small airways (110, 153, 166). The general approach has been to place multiple single-path trumpets of different size in parallel. These models have been particularly effective in describing the progressively increasing slope of phase III during a multiple breath washout (MBW) of a gas such as nitrogen. Multiple breath washout is a lung function test that is used to examine ventilation distribution and gas mixing in the airways and alveolar regions of the lungs. In one technique, subjects tidal breathe pure O_2 while a gas analyzer measures nitrogen concentration during exhalation, tracking the nitrogen washout from the lungs (multiple breath nitrogen washout, MBNW, Fig. 6A).

During the MBNW, the normalized slope of phase III progressively increases with each tidal breath. The phase III slope of each exhalation is normalized by the mean concentration of the gas over the region of analysis (typically 50%-90% of the exhaled volume, Fig. 6B). The normalized slope ($S_{N,III}$) is then plotted versus lung turnover (cumulative exhaled volume divided by the functional residual capacity, Figure 6C), and information related to airway and alveolar gas mixing can be extracted (88, 121, 122, 166).

Mathematical models demonstrate that $S_{N,III}$ for early breath numbers is controlled by diffusion and convection-dependent inhomogeneities, while $S_{N,III}$ for later breath numbers is controlled by convection-dependent inhomogeneities (111). This modeling is more comprehensive and explains

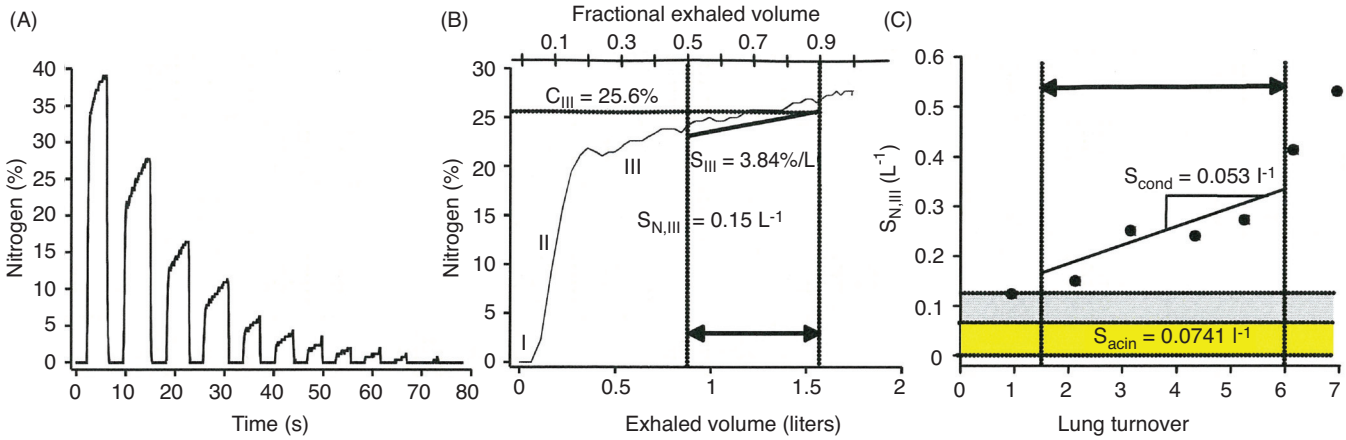

Figure 6 Multiple breath nitrogen washout. The nitrogen in the lungs is progressively washed out over the course of 10 to 20 breaths of inspiring pure oxygen (**A**). Each tidal exhalation results in an exhalation profile represented by three phases (**B**). The slope of phase III (S_{III}, change in concentration divided by change in exhaled volume) is determined by linear regression over the region spanning 50% to 90% of the exhaled volume for each breath and provides information on ventilation inhomogeneities. In general, the normalized phase III slope increases with lung turnover (cumulative exhaled volume normalized by the functional residual capacity) or breath number. The normalized phase III slope, $S_{N,III}$ (**B**), is S_{III} divided by the mean concentration over the same region, C_{III}, and can be plotted as a function of lung turnover (**C**). Then, theoretical calculations demonstrate that the rate of increase in $S_{N,III}$ with lung turnover over the range of 1.5 to 6.0 provides an index of ventilation inhomogeneities in the proximal or conducting airways (airway generations 1-16) (**C**). This index is denoted S_{cond} (L^{-1}). Furthermore, an index of ventilation inhomogeneity in the acinar region (airway generations 17-23) can be extracted from $S_{N,III}$ in the first breath (after subtracting the component due to S_{cond} – height of gray shaded region and equal to S_{cond} multiplied by lung turnover for the first breath) (**C**). This index is denoted S_{acin} (L^{-1}) – height of yellow shaded region. As ventilation inhomogeneity increases in the respective regions of the lungs, S_{cond} and S_{acin} increase.

how the two distinct segments of the $S_{N,III}$ plot (Fig. 6C) represent inhomogeneities in different regions of the lung; S_{acin} is an index of ventilation inhomogeneity in the acinar airways, while S_{cond} is an index of inhomogeneity in the conducting airways (Fig. 6C).

Additional models, which require numerical solution of the Navier-Stokes equation of motion, describe mixing patterns at airway bifurcations. These models have potential utility in understanding drug and air pollutant deposition patterns during inhalation, as recently reviewed (80, 81). More recently, improvements in the resolution of computed tomography and computing speed have allowed detailed three-dimensional reconstruction of *in situ* human airway tree anatomy down to generation 6. The reconstructions have been used to create a numerical mesh for simulations of anatomically based airway gas mixing and particle deposition (69, 105).

Experimental

Experimental models of airway gas exchange include both physical and mammalian models. In humans, experimental models have been limited to two major classes: (i) single exhalation gas profile or (ii) inspiration of a prescribed bolus of gas (volume less than the volume of the airway tree) followed by expiration of the same volume. The application of the single exhalation gas profile is normally limited to an endogenously produced gas that appears in the exhaled breath. The profile can be typically characterized by three phases (Fig. 6B). Phase I represents the emptying of the volume of air that does contain any of the gas of interest and thus represents the region of the lungs that does not contribute toward gas exchange; hence, phase I is commonly referred to as the dead space. Phase II is a volume of gas representing the transition from the dead space. The region of the lung that actively participates in gas exchange, or phase III, which represents air that originated in the alveolar region but has traversed the airway tree upon exhalation and can thus be altered or conditioned by the airways during exhalation. As a result, the exhalation profile is useful to characterize the exchange of gases with both the alveolar region and the airways.

Analysis of the single exhalation gas profile includes both nonparametric and parametric features. Nonparametric characteristics of each region include the mean concentration and the volume. Simple parametric features based on statistical models include the coefficient of variation and the normalized (by the mean concentration) slope from linear regression. These end points can provide a robust means of detecting intersubject and intergas differences. For example, a gas such as NO has a smaller dead space volume than CO_2 and a negative phase III slope (see section "Exchange of Nonrespiratory Gases" below) (159). Numerous factors can influence the shape of the exhaled profile of a gas including, but not limited to, inhalation flow, exhalation flow, inhalation volume, exhalation volume, solubility, preexpiratory breathhold, inspired temperature, inspired humidity, and preinspiratory respiratory rate. All of these factors influence one or more of the physical determinants of airway gas exchange as described in section "Physical Phenomena Governing Airway Gas Exchange."

A more specific experimental model in humans to probe the exchange of either an endogenous gas or an exogenous gas with the airway tree is the bolus-response method. In brief, a small volume of gas whose concentration profile (gas concentration as a function of volume or time) is known or prescribed is inspired only into the airway tree and then expired with or without a breathhold. The concentration profile of gas in the expired bolus is measured and compared to the inspired profile. As with the single exhalation profile, both nonparametric and parametric indices can be applied for quantitative characterization. For example, the total volume of gas inspired or expired (nonparametric) can be determined by simply integrating the area of the curve. Additional parametric indices can be estimated by regressing physiologically based mathematical models to the gas concentration profile. This approach can be useful to determine either the anatomical site of gas exchange (38, 58, 59, 103) or the rate of bronchial blood flow (109, 135, 168).

Animal models to probe airway gas exchange include those described for humans (single exhalation and bolus-response) and also include more invasive procedures. For example, in larger animals (e.g., canine or ovine), the trachea can be isolated, with the circulation intact, and the animal is ventilated posterior to the isolation near the carina (150, 154). A controlled flow (rate and concentration) of air can be passed through the trachea whereby gas exchange with the tracheal wall occurs. The gas of interest can be delivered through the bronchial circulation and the rate of desorption to the gas stream is observed; conversely, the gas can be delivered in the inlet airstream and absorption by the tracheal wall is observed. This method has the advantage of utilizing a wider range of gases, with more precise control over flow and physical parameters such as gas exchange surface area.

Physical models of airway gas exchange include construction of a single tube or a network of bifurcating tubes to simulate mixing and absorption or desorption of a gas or can be combined with cells to characterize gas phase release. For example, cast models of the upper respiratory tract of humans can be constructed and used to determine mass transfer coefficients (54). Conversely, both a single tube using oscillatory flow or a network of connected tubes simulating the symmetric bifurcating structure of the airways has been used to determine effective gas phase diffusivities (47, 132). More recently, primary human airway epithelial cells have been cultured at an air-liquid interface and the rate of NO gas phase release is quantified (63, 152). Physical models provide precise control over parameters such as surface area, branching angle, and volumes.

Exchange of Nonrespiratory Gases

The transport of gases can be categorized by their source and their chemical reactivity. For example, a gas can be produced

by the body (*endogenous*) and transported to the environment (*exogenous*), or vice versa. Furthermore, an exogenous gas can exchange with the airway tree through inspiration (e.g., air pollutant) or following ingestion and transport to the airways through the blood (e.g., ethanol). A gas can be considered chemically *reactive* if the transport process within the airways involves a significant chemical reaction(s), otherwise it is considered chemically *inert*. Because the airways are lined by a thin layer of water that is ~95% water by weight, the solubility of a gas in water ($\lambda_{i,w}$) is also a convenient physical property that dictates gas exchange properties in the airways. While solubility is a spectrum, gases can be characterized as high solubility ($\lambda_{i,w} > 1000$), moderate solubility ($0.1 < \lambda_{i,w} < 1000$), or low solubility ($\lambda_{i,w} < 0.1$). There are numerous gases that have been reported to exchange with the airways. Below is a description of several prominent examples that fall into the different categories.

Water (endogenous, inert, high solubility)

A major function of the upper respiratory tract and large airways is humidification of the inspired ambient air to protect the delicate alveolar tissue from drying. This process is simply the exchange of water vapor (gas phase of water) between the airway wall and airstream and thus represents the exchange of an endogenous inert gas. The solubility of water in water itself is simply the vapor pressure of water at any given temperature. At 37°C, the vapor of water is 47 mmHg, which corresponds to $\lambda_{w:w} \cong 10{,}000$. During inspiration of air that is not saturated (and normally cooler than body temperature), the partial pressure of water lining the airways is larger than that in the airstream, creating a gradient for transfer of water from the airway wall and into the airstream. Water will be transported until the airstream is saturated with water at the temperature of the airway wall (34-37°C). The point of saturation during normal tidal breathing is approximately airway generation 5 (Fig. 7), based on both experimental (32, 62) and modeling studies (49, 55, 160). There is marked humidification occurring in the nasal cavity (for nasal breathing) or oral cavity (for oral breathing) and then again in the upper bronchi with minimal water exchange occurring in the pharynx and trachea. Marked changes in the ventilation rate, as that might occur during exercise, can impact the point of saturation, but the air entering the alveolar region is fully saturated and warmed to body temperature under essentially all conditions. Thus, water exchange occurs entirely within the airway tree and not within the alveolar region.

Ethanol (exogenous ingested, inert, high solubility)

Ethanol appears in the exhaled breath following ingestion of alcoholic beverages. It is metabolized in the liver, but not in pulmonary cells, with solubility $\lambda_{e:w} \cong 2500$ (65). Thus, ethanol is an example of an exogenous, inert, high-solubility gas. The physiological relevance of ethanol exchange lies primarily in the interpretation of the alcohol breath test as a noninvasive means of determining blood ethanol levels. There is a rich experimental literature measuring exhaled ethanol profiles in an effort to understand the physiological principles that impact the concentration in the exhaled breath and how this concentration is related to the concentration in blood. Experimental profiles have a positive phase III slope (Fig. 8A), but the magnitude of the slope is independent of the exhalation flow (48). Furthermore, hyperventilation or hypoventilation before performing a single exhalation can decrease and increase, respectively, the concentration of ethanol at end exhalation by as much as 55% (107); similarly, breathing dry cold air or warm moist air before performing a single exhalation can significantly decrease the concentration of ethanol by up to 10% (64).

In an effort to understand the experimental observations, mathematical models describing the simultaneous exchange of heat, water, and ethanol have been developed (3,48,160,161). The modeling work utilized the Weibel symmetric bifurcating tree and then considered each airway as a series of annuli representing the mucous layer, the epithelium, the lamina propria, and the surrounding blood from the bronchial circulation. The latter serves as the source (following ingestion) and constant concentration. Figure 8B is an example of a control volume through the airway wall used in model simulations, and Figure 8C is the flux of ethanol from the airway generations during a single exhalation following inspiration to total lung capacity. Note that the flux is bimodal

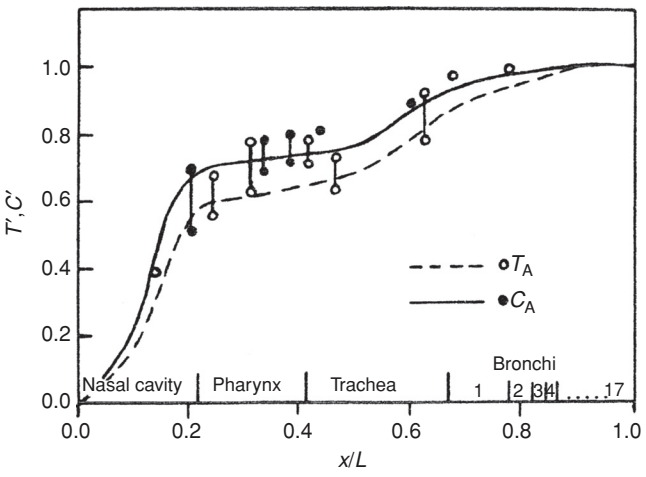

Figure 7 Water and temperature profiles in the airway tree. Predicted nondimensional inspiratory temperatures and water vapor concentration profiles during room air breathing at rest plotted as a function of the nondimensional distance, *x/L*. Room air breathing at rest is defined as an inspiratory flow rate of 300 ml/s, an inspiratory temperature of 23°C, and a relative humidity of 30%. The blood temperature is set at 32°C in the nasal cavity, rising linearly distal to the nasal cavity at a rate of 0.33°C/cm, reaching body core temperature near the carina. Superimposed are the values of air temperature, T_A and C_A determined experimentally within the human respiratory tract by various researchers. The characteristic length used to nondimensionalize the distance into the airways is measured from the nose to the 18th generation of the Weibel lung (169). From reference 55.

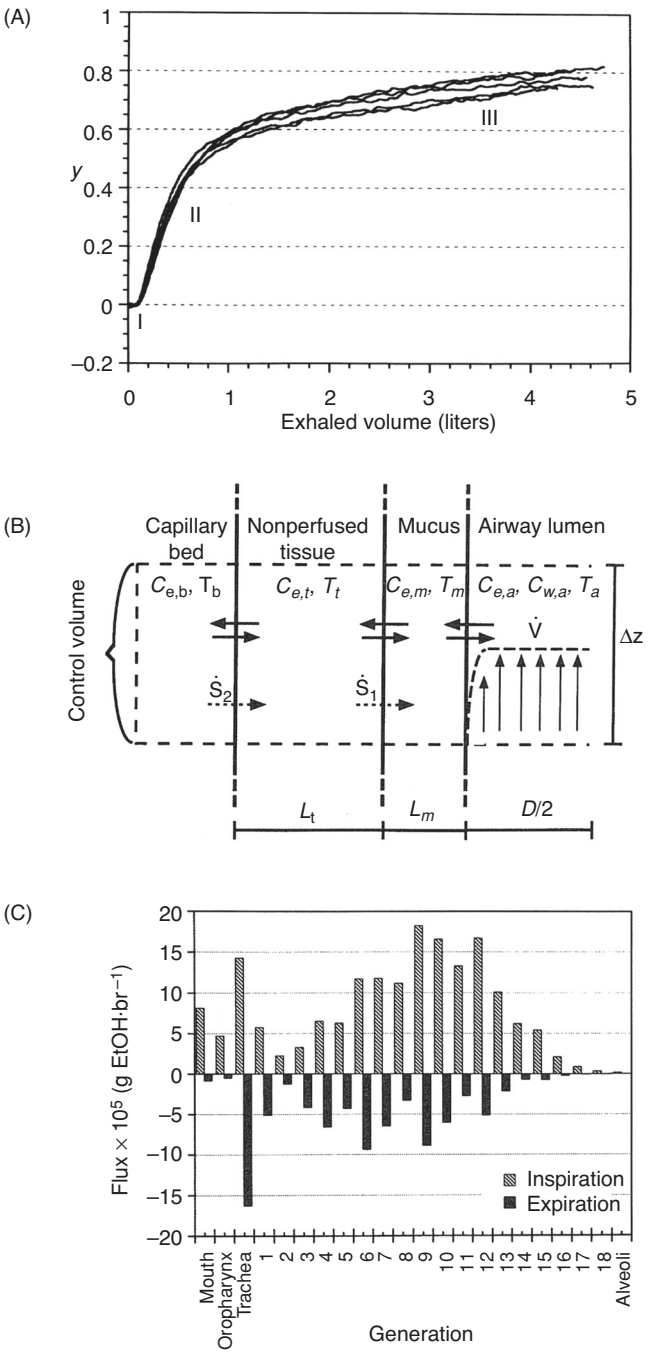

Figure 8 Exhaled ethanol. (**A**) Experimental exhaled ethanol profiles from healthy adult subjects. The *y*-axis is the breath ethanol concentration normalized by the blood ethanol concentration. Note the presence of three phases in the exhalation profile. (**B**) Control volume used for mass and energy balances in a mathematical model of simultaneous heat, water, and ethanol exchange in the airways. Ethanol source is the blood (right-hand side). The ethanol can then diffuse through the layers of the airway wall before entering the gas phase of the airway lumen. (**C**) Steady-state mathematical predictions of the flux of ethanol from different regions of the upper and lower respiratory tract during tidal breathing (both inspiration and expiration). A positive flux denotes transport of the ethanol from the surface to the airstream. From reference 48, 49.

and thus similar to water. There is a significant flux of ethanol in the oral cavity/trachea, and a second peak in generations 8 to 12. The bimodal distribution is due to the balance between a decreasing gradient between the airway wall and gas stream and the progressively increasing surface area of the airway tree. Also of interest is that ~50% of the ethanol that is absorbed by the inspired air is deposited back to the airway wall (desorbed) on expiration. This phenomenon is due to a lowered concentration of ethanol in the mucous layer following transport during inspiration and the fact that the airstream is fully saturated at body temperature when exiting the alveolar region on expiration; thus, there is a gradient leading to the transport of ethanol from the airstream to the airway wall (49). Thus, because of the high water solubility, the exchange of ethanol is entirely within the airway tree and not the alveolar region.

Although the vast majority of experimental and theoretical work has focused on ethanol airway exchange as an exogenous gas, recent experimental work has detected ethanol in the exhaled breath at much lower concentrations under basal conditions and significantly elevated levels (but still far below that following the ingestion of ethanol) following consumption of glucose (44). The concentration of ethanol in the breath tracks closely with the pattern of blood glucose and may be due to anaerobic metabolism of bacteria in the gut. Nonetheless, endogenously produced ethanol may be a useful biomarker related to blood glucose, but the interpretation depends on understanding gas exchange dynamics in the airways.

Nitric oxide (endogenous, reactive, low solubility)

Exhaled NO was first detected in the exhaled breath by Gustafsson et al. in 1991 (53). Since then, there have been many reports under many different conditions including disease states and exercise. Early reports utilized mixed expired and end-tidal samples and reported values of 8 to 15 ppb (20). As the instrumentation improved, more sophisticated breathing maneuvers were possible including the dynamic shape of the exhalation profile (118, 159). Breathholding significantly increased the peak value of NO from ~3 ppb to over 100 ppb following a 60-s breathhold. In addition, the NO profile had a significantly different shape when compared to CO_2. After reaching an initial peak, the concentration of NO began to decrease and thus was not a monotonically increasing function of exhaled volume. Perhaps, the most significant finding was the marked dependence of the concentration on exhalation flow (Fig. 9) (143). This was consistent with the large peak in phase I following breathhold. Other factors that impact the interpretation of exhaled NO include the nasal cavity (primarily the paranasal sinuses) as a major source of NO (37, 75, 79) and a diet rich in nitrate (108).

NO is synthesized *in vivo* from enzymatic degradation of L-arginine to L-citrulline, is a free radical and thus chemically reactive due the presence of 11 valence electrons, and

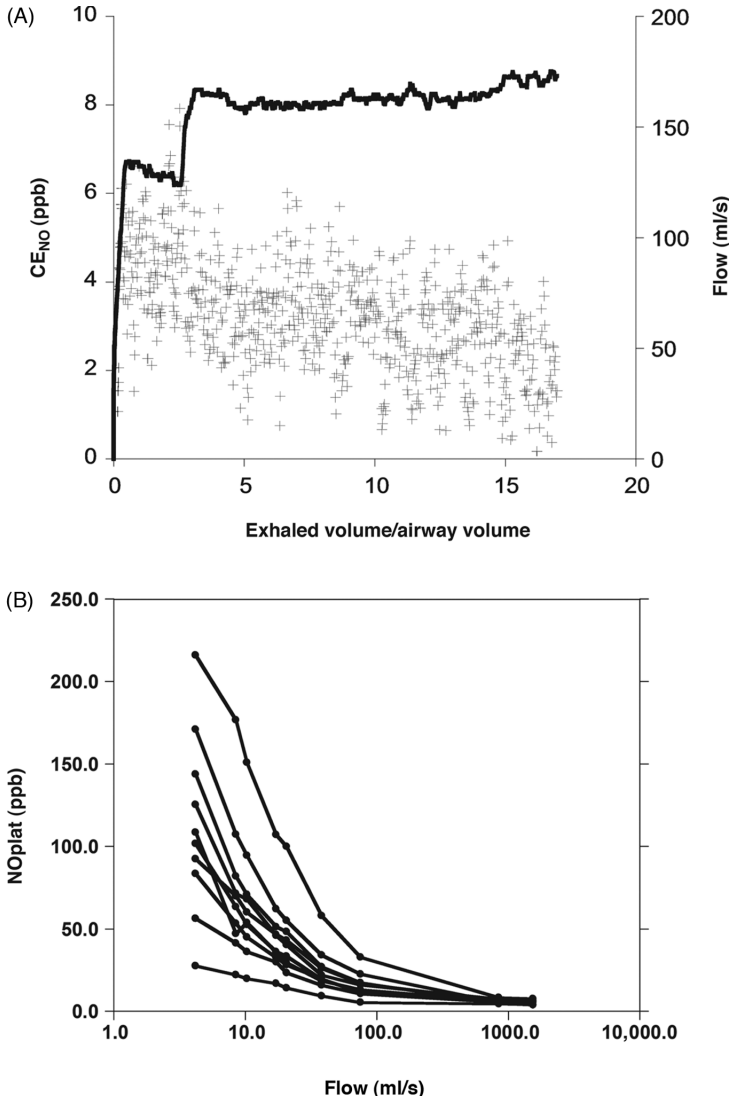

Figure 9 Exhaled nitric oxide. (**A**) experimental exhaled NO profile and exhalation flow in a healthy adult subject. Note the slightly negative slope of the NO concentration with exhalation volume even when the flow is constant. The mean concentration over a specified volume or time interval is denoted by the plateau concentration (NO_{plat}). (**B**) Experimental exhaled nitric oxide concentrations from the plateau region of the profile (NO_{plat}) are plotted as a function of the constant exhalation flow for 10 healthy adult subjects. Note the strong inverse dependence between exhaled NO concentration on flow and the significant intersubject variability. From reference 30, 143.

has a solubility of $\lambda_{NO:w} \cong 0.04$. Thus, NO would be considered an endogenous, reactive, low-solubility gas. The enzyme is nitric oxide synthase (NOS) for which there are three isoforms (46). Two forms are expressed constitutively (neuronal or nNOS and endothelial or eNOS), and the third is inducible (iNOS). NOS activity has been identified in a variety of pulmonary cells including macrophages (66), neutrophils (127), mast cells (19), fibroblasts (67), vascular smooth muscle cells (26), endothelial cells (61), and bronchial epithelial cells (82). Each of these cell types represents a possible source of NO in the exhaled breath, although the proximity of the epithelial cell to the airway lumen and the upregulation of iNOS in asthmatic subjects within the epithelial cell make it the most likely source. NOS is the likely source of exhaled NO, as inhalation of competitive inhibitors (i.e., L-NAME, L-NMMA, or aminoguanidine) of NOS decrease exhaled NO levels (35, 84, 125, 129, 130, 172, 173). It is possible that degradation of GSNO by enzymatic or nonenzymatic pathways is also a source (42, 93), but GSNO is likely an intermediate reservoir for free NO produced from NOS.

NO reacts readily with several molecules present in biological systems including molecular oxygen (and subsequently water), superoxide, thiols, and metalloproteins (including heme and nonheme). The *in vivo* half-life has been

estimated to be 0.1 to 10 s depending on the local concentration of specific substrates. The reaction rate constants for many of these reactions have been measured and have been recently incorporated these into a microscopic model on NO transport from the epithelial cell, through the mucus layer, and into the gas phase (139, 141, 158). The rate of consumption may be altered in disease states such as asthma and cystic fibrosis (CF) where larger concentrations of superoxide are present.

Experimental evidence clearly demonstrates that NO exchange dynamics are unique based on production within the airway cells and potentially consumption due to several substrates. Hence, previous mathematical models to understand exchange principles of gases such as carbon dioxide, nitrogen, oxygen, and water are inadequate. Since 1998, numerous research groups have made significant contributions toward our fundamental understanding of NO exchange dynamics in the lungs through not only the creation of mathematical models but also new experimental algorithms to test, validate, and characterize the model parameters.

The observation that exhaled NO concentration is inversely related to the exhalation flow is consistent with a fixed volume source; that is, as exhalation flow increases, the contact time of the airstream with a surface serving as the source of NO would be reduced creating an inverse dependence on the flow. Hence, the relatively rigid conducting airways are a plausible source of NO in the exhaled breath. If the airways were the only source of exhaled NO, then one would predict that the product of exhaled NO concentration and flow (i.e, elimination rate of NO) would be constant over a wide range of flows; however, early experimental observations demonstrated that the elimination rate of NO was a positive function of exhalation flow (159). This observation was consistent with the source of NO from a region of the lung that changes volume during exhalation. In other words, the observation that the elimination rate of NO was a positive function of exhalation flow was consistent with a source of NO in the alveolar region. These principles formed the foundation of the two-compartment model (i.e., an airway compartment and an alveolar compartment) of NO exchange, first reported in 1998 (Fig. 10) (157) and later confirmed by four additional independent research groups (56, 68, 119, 144).

In the simplest form, the two-compartment model can be characterized by two parameters: a maximum flux of NO from the airway compartment ($J_{aw}'_{NO}$, pl/s, airway generations 1–16) and a steady-state mean distal airway/alveolar concentration of NO (CA_{NO}, ppb). A series of experimental algorithms characterized by collecting exhaled NO concentration at different constant exhalation flows has been presented and reviewed (50). While the simplicity of the initial two-compartment model is a tremendous strength, recent work has demonstrated that axial diffusion of NO in the gas phase cannot be neglected (137, 138, 140, 165). Incorporating axial gas-phase diffusion of NO produces a two-compartment model with more complex governing equations and modified algorithms to characterize $J_{aw}'_{NO}$ and CA_{NO} (30, 73). For example, a simple method used widely to determine $J_{aw}'_{NO}$ and CA_{NO} is to regress a line through a plot of the elimination rate of NO versus the exhalation flow, and the intercept and the slope are estimates of $J_{aw}'_{NO}$ and CA_{NO}, respectively ("slope-intercept" method) (159). When axial diffusion of NO in the gas phase is considered, NO from the airway tree diffuses back ("back diffusion") into the alveolar region where it can falsely elevate the estimate of CA_{NO} and depress the estimate of $J_{aw}'_{NO}$. Thus, the modified algorithm based on the slope-intercept method still uses the slope to estimate CA_{NO} but subtracts a term proportional to the airway flux to account for axial diffusion; similarly, the estimate for $J_{aw}'_{NO}$ remains the intercept but is multiplied by a factor to account for the loss to the alveolar region (30).

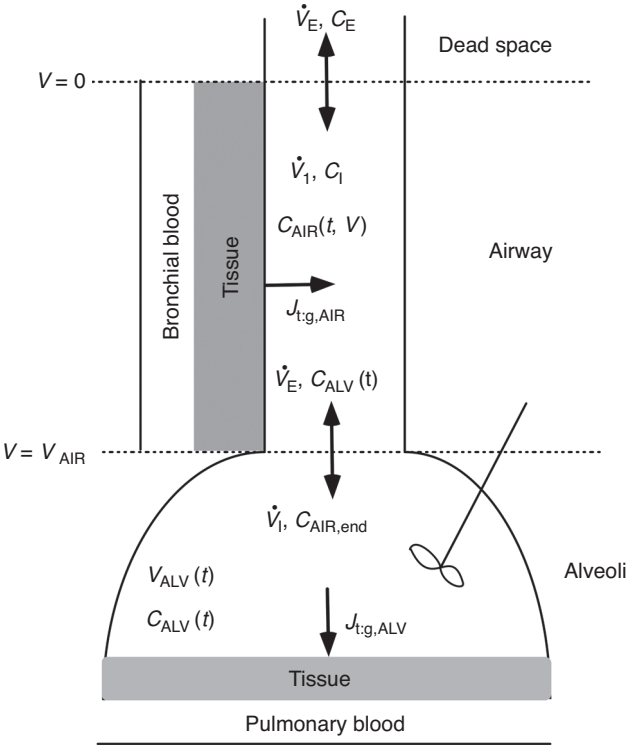

Figure 10 Two-compartment model of nitric oxide (NO) exchange. Schematic of two-compartment model for NO pulmonary exchange. First compartment represents relatively nonexpansile conducting airways; second compartment represents expansile alveoli. Each compartment is adjacent to a layer of tissue that is capable of producing and consuming NO. Exterior to tissue is a layer of blood that represents bronchial or pulmonary circulation and serves as an infinite sink for NO. E and I, expiratory and inspiratory flow, respectively; C_E and C_I, expiratory and inspiratory concentration, respectively; C_{AIR} and C_{ALV}, airway and alveolar concentration, respectively; V_{AIR} and V_{ALV}, airway and alveolar volume, respectively; $J_{t:g,AIR}$ and $J_{t:g,ALV}$, total flux of NO from tissue to air and from alveolar tissue, respectively; t, time; V, volume. From reference 157.

Ozone (exogenous, reactive, low solubility)

Ozone (O_3) is present in the stratosphere and plays a critical role in controlling exposure of the earth's surface (troposphere) to ultraviolet radiation. Significant attention to "ozone

depletion" in the stratosphere has led to numerous changes in the regulated use of chemicals such as fluorocarbons. However, this source of ozone is distinct from the ozone present in the troposphere, which is the product of chemical reactions involving volatile organic compounds and oxides of nitrogen in the presence of ultraviolet light. Hence, the concentration of tropospheric ozone depends strongly on the local combustion of fossil fuels and exposure to sunlight and therefore tends to be highest during the day and during the late spring through early autumn. As a free radical, ozone is highly reactive with numerous substrates and has a low solubility in water ($\lambda_{O_3:w} \cong 1.3$); thus, ozone is an example of an exogenous, reactive, low-solubility gas that exchanges with the airways.

Ozone exchanges with the airways because of its high chemical reactivity. In particular, ozone reacts with lipids present in the epithelial cell membrane leading to peroxidation. Lipid peroxidation can lead to an increase in epithelial cell membrane permeability and an inflammatory response involving the recruitment of neutrophils (13) that can lead to the release of proinflammatory mediators such as interleukin-8. The clinical consequences of the ozone exposure depend strongly on the concentration and time of exposure. Acute exposure of less than 0.12 ppm has little or no consequence (85), but longer term exposures of concentrations as low as 0.08 for up to 8 h can lead to cough, substernal chest pain, and decreases in lung function as determined by a decrease in forced expiratory volume in one second (FEV_1) (164). As a result, concentrations of ozone in the ambient air are regulated by the Environmental Protection Agency and the current threshold is 0.08 ppm over an 8-h window.

Early modeling work of ozone exchange utilized the Weibel symmetric bifurcating structure of the airway tree with a classic convection-diffusion equation that included a chemical consumption term in the airway lining (98). This study could predict significant uptake of ozone in the tissue compartment of the small airways (peak in generations 12–16), but the theoretical predictions were highly dependent on the rate of chemical consumption, mass transfer coefficients, and the physical size (e.g., thickness) of the tissue and airway compartments. To test these predictions, the bolus-response method has been used extensively to quantify the location and extent of exchange of ozone with the airways including the effects of nasal breathing, respiratory rate, smoking, and coinhalation with other gases (8, 14, 24, 25, 58, 59, 126). For example, during oral tidal breathing, the fraction of total ozone inhaled in the bolus absorbed by the airways increases approximately linearly with penetration volume (the volume that the bolus is allowed to penetrate during inspiration). Importantly, the absorbed fraction approaches 1.0 before entering the respiratory airways, indicating nearly complete exchange of ozone with the airways (Figs. 11A and 11B). The rate of absorption decreases as flow increases due to a shorter residence time within the airway tree.

Exhaled Biomarkers

The exhaled breath has long been considered a valuable source of "biomarkers," that is, molecules whose presence and concentration reflect biological activity within the lungs as well as peripheral tissues. The best understood are the respiratory gases, CO_2 and O_2, which mark respiration of metabolizing tissues. However, there are literally thousands of additional compounds in the exhaled breath. The challenge facing the field of exhaled biomarkers is twofold: (i) reliable and affordable detection and (ii) interpreting the link between the concentration of the biomarker and the biology underlying its generation. Below is a brief description of several examples of exhaled biomarkers that represent different extremes in our ability to detect and interpret.

Respiratory gases (CO_2 and O_2)

The respiratory gases, CO_2 and O_2, are the most basic examples of exhaled biomarkers. Their presence in the exhaled breath can be easily (reliable and affordable) measured and the interpretation is well characterized. During inspiration, ambient air normally contains 21% oxygen by volume and 79% nitrogen along with trace amounts of many gases including CO_2. As air enters the alveolar region, O_2 diffuses into the pulmonary blood and CO_2 diffuses out of the blood and into the gas stream. The expired air contains approximately 16% O_2, 5% CO_2, and 79% nitrogen, as well as many additional trace compounds that reflect additional metabolic or biological activity. Essentially all respiratory gas exchange occurs in the alveolar region due to the low water solubility of O_2 ($\lambda_{O_2:w} \cong 0.08$) and CO_2 ($\lambda_{CO_2:w} \cong 3$). It is also evident that the concentration and the change in concentration following a respiratory cycle of the respiratory gases are much larger than other biomarkers, which reflects the major function of the lungs. For these reasons, the detection and interpretation of exhaled O_2 and CO_2 are relatively straightforward.

Nitric oxide

Some of the earliest observations connecting NO with asthma pathobiology were measurements of NO in the exhaled breath (2, 78) approximately 13 years ago. These observations demonstrated that NO was a noninvasive biological marker, was significantly elevated (~three- to fourfold) in mild untreated asthma, could be reduced to near normal levels following corticosteroid therapy, and likely reflected the inflammatory status of the lower airways (as opposed to bronchodilatory status) (2, 7, 45, 76-78).

These initial exciting studies prompted many new investigations, at both basic science and clinical levels, in an attempt to better understand the source and potential clinical utility of the exhaled NO signal. Several landmark studies demonstrated the complexity and uniqueness of exhaled NO relative

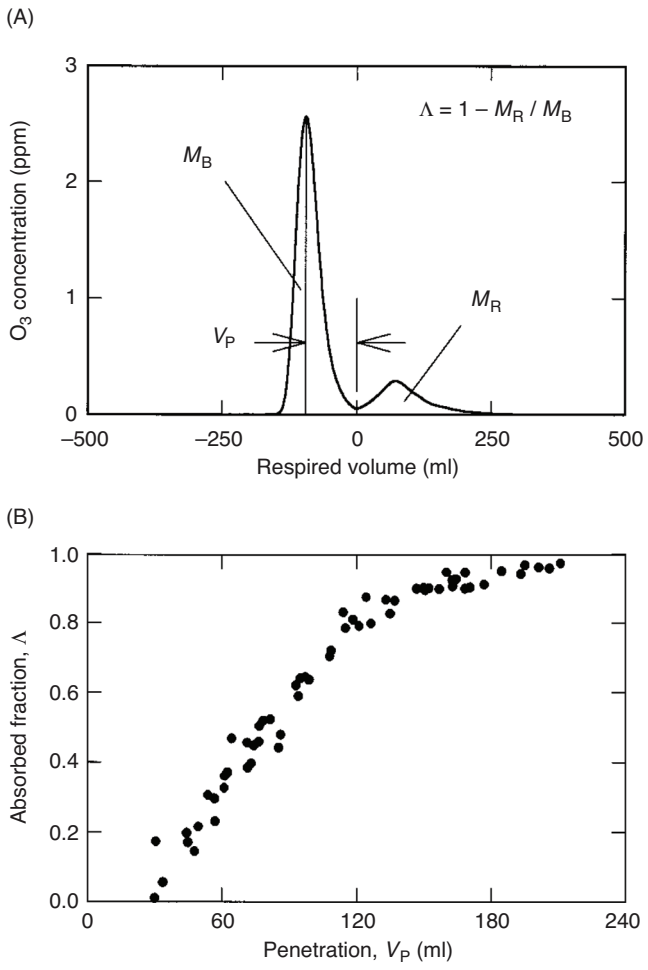

Figure 11 Ozone (O_3) absorption in the airway tree. Concentration curves from an O_3 bolus test breath (**A**) and Λ-V_P distribution from one subject (**B**). Absorbed fraction (Λ) represents amount of O_3 that does not reappear during exhalation relative to amount inhaled, and penetration V_P represents mean airway volume traversed by O_3 molecules during inhalation, if they were not absorbed. M_B and M_R, amounts of O_3 inhaled and exhaled, respectively. From reference 24.

to other endogenous gases (e.g., CO_2 and N_2) such as a significant dependence on exhalation flow that could be attributed to a substantial airway source (56, 119, 142-144, 157, 159), a significant nasal component (79, 96), as well as an oral component (108).

Numerous correlative studies with other biological and physiological markers followed with mixed results. Some suggested that NO reflected the inflammatory status by correlation with eosinophila in peripheral blood (12, 128, 145-147, 151) and sputum (16, 97, 106, 115), while others did not (22,89-91,116,156). There were also inconsistent reports as to whether exhaled NO correlated with spirometry, with some studies finding a correlation (92, 145) and others could not (33, 90, 106, 147, 151).

Several more recent longitudinal studies suggest that exhaled NO can either be used to diagnose asthma (15, 39) or be an effective noninvasive index of asthma control and thus be used to titrate the dose of, or predict the response to, corticosteroids (120, 148, 155). However, at least one longitudinal study demonstrated that exhaled NO was not predictive in reducing the dose of corticosteroid (87).

Another important feature of exhaled NO is the significant variability reported within a group of similar individuals (e.g., healthy controls, asthma, CF). As with most biological signals, exhaled NO demonstrates a log-normal distribution. At a constant exhalation flow of 50 ml/s (American Thoracic Society guidelines), the geometric mean value in healthy children (age 4–17 years) is 9.7 ppb, but the upper end of the 95% confidence interval is 25.2 ppb (23). A large range of values in clinically similar groups of asthmatic subjects is also invariably reported. These findings strongly suggest that our knowledge of the underlying source and determinants of exhaled NO remain crude.

Despite the limitations and inconsistencies in the literature regarding exhaled NO, there remains substantial interest and momentum in the clinical realm to use NO as a noninvasive index of inflammation. However, there remain many unanswered fundamental questions. At the most basic level,

we still do not know exactly what the exhaled NO signal is marking or why the magnitude of the signal is so variable among clinically similar subjects. The NO signal must, however, reflect the underlying metabolism of nitrogen species in the epithelium.

pH

Exhaled air is saturated with water and contains numerous metabolites that are in liquid phase at body temperature and thought to reflect the composition of the small respiratory airways due to the presence of a surfactant (1). One example is the presence of hydrogen ions (H^+), whose concentration determines the pH of the exhaled breath condensate and thus reflects the pH of the lower airways. The water vapor in the exhaled breath can be condensed through cooling, and when properly aerated to eliminate effects on the pH from *ex vivo* exposure, the pH can be determined (60).

It was first reported in 2000 that the pH of the exhaled breath condensate during acute asthma was more than 2 log orders lower than healthy controls and that corticosteroid therapy returned the pH to normal levels (60). Numerous additional studies have reported similar results (27, 28, 83, 123). Airway acidification can significantly alter the chemistry of nitrogen oxide species such as the protonation of nitrite (NO_2^-, $pK_a = 3.4$) to form nitrous acid, which decomposes to release NO. Furthermore, low airway pH can reduce ciliary beat frequency (95), increased the mucous viscosity (57), stimulate ion channels in capsaicin-sensitive neurons and thus bronchoconstriction (17), and is correlated with sputum eosinophilia (83). Thus, while the mechanism leading to a low airway pH in acute asthma is not known, it is clear that the observed acidification can impact airway function. In addition to asthma, it has now been demonstrated that other lung diseases, including chronic obstructive pulmonary disease (COPD) (83) and CF (27, 102), have alterations in the pH of the exhaled breath condensate. These studies have correlated the lower pH of the breath condensate with other markers of oxidative stress, including hydrogen peroxide and 8-isoprostane (11, 83, 99), that are elevated in inflammatory lung diseases.

Volatile organic compounds

The presence and physiological relevance of biomarkers such as NO and pH have stimulated research activity aimed at identifying other potential useful biomarkers. In particular, it has been known for decades that numerous volatile organic compounds (VOCs) are present in the exhaled breath (9, 43) and likely reflect relevant systemic and pulmonary metabolic processes. Several prominent examples include acetone, ethane, and pentane.

Acetone is a high-solubility gas ($\lambda_{acet:w} \cong 250$) that is produced endogenously through several metabolic pathways. It has been known to be present in the exhaled breath since the mid-19th century and thus has a long history of investigation as an exhaled biomarker. The metabolic features of acetone in mammals have been recently reviewed in detail (70) and thus only a short summary will be presented. Acetone can be produced by two pathways: (i) decarboxylation of acetoacetate and (ii) dehydrogenation of isopropanol. The major source in mammals is the former and results during the breakdown of lipids or proteins. Thus, blood acetone levels have been known to be elevated in metabolic conditions that favor degradation of lipid or protein for energy such as subjects with diabetes (44, 101), congestive heart failure (86), or fasting (149). Thus, the use of acetone as a breath biomarker has significant potential to monitor prevalent diseases. The high solubility of acetone results in significant airway gas exchange, which has been reported both experimentally and in physiologically based models of acetone production and excretion through the exhaled breath (6, 100, 154). The analytical methods to measure acetone have generally relied on mass spectrometry (6, 162), which is rapid enough to generate the dynamic shape of the exhalation profile (Fig. 12). The exhalation profile displays features, including phase II and a positive sloping phase III, that are similar to other exhaled breath markers.

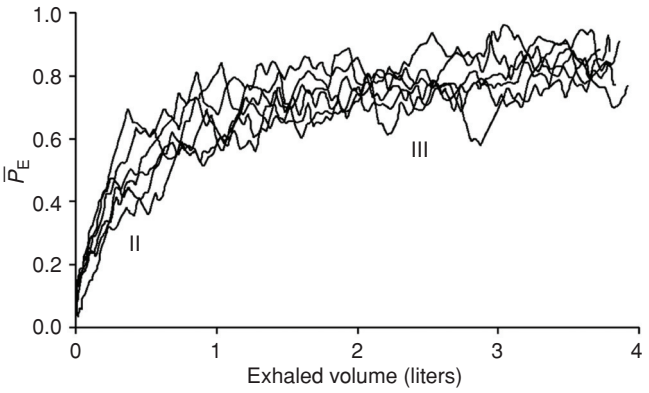

Figure 12 Exhaled acetone profile. Repeated (six times) single exhalation expirograms, using mass spectrometry, for acetone are shown for a single health adult subject. The concentration in the exhaled breath is normalized by the concentration in the alveolar region determined through isothermal rebreathing. Lag time of the instrument and dead space in the collection apparatus have been accounted for, and note the lack of a phase I indicative of zero dead space and thus significant airway gas exchange. Phase II and a positively sloping phase III, similar to ethanol and other breath biomarkers, are evident. From reference 6.

Ethane and pentane are low-solubility gases ($\lambda_{eth:w} \cong 0.1$; $\lambda_{pen:w} \cong 0.03$) that are also products of lipid metabolism, specifically lipid peroxidation of the cell membrane. As such, they are thought to represent markers of oxidative stress in the lungs as well as other tissues. For example, elevated ethane levels in the exhaled breath have been detected following reperfusion injury in an ischemic liver model (72), COPD (114), asthma (113), intense exercise (171), scleroderma (31), and interstitial lung diseases (71). All of

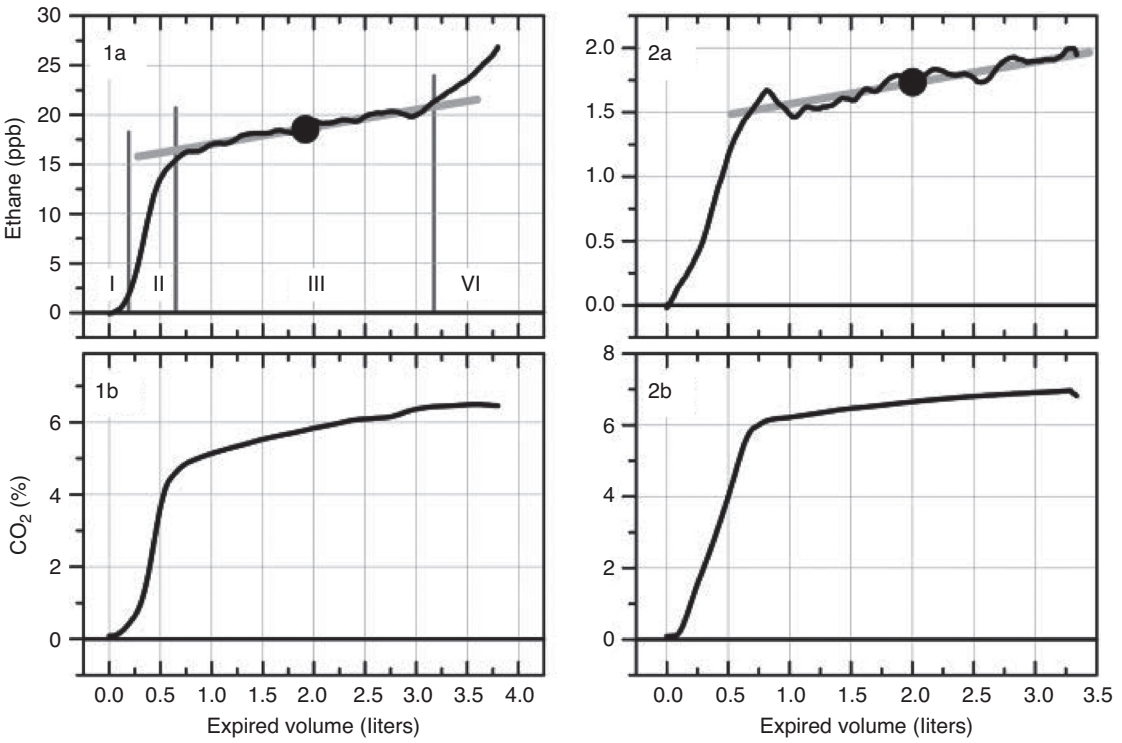

Figure 13 Exhaled ethane profile. Recorded single exhalation expirograms for ethane and CO_2. 1a and 2a: expirograms for ethane at a scale of 30 and 2 ppb, respectively. 1b and 2b: corresponding expirograms for CO_2. In 1a, three phases (I-III) of expiration are marked. The additional phase IV belongs to exhaled breath beyond the functional residual volume. The gray line represents a linear regression, which is used to determine the slope of the alveolar plateau. The mean alveolar concentration is labeled with a dot. From reference 167.

these conditions are associated with oxidative stress and inflammation, and corticosteroid therapy can reduce ethane concentrations in some conditions (113, 114). Interest in assessing ethane in the exhaled breath has prompted the development of new analytical techniques that are more rapid including laser spectroscopy capable of measuring the exhaled ethane single exhalation profile (167) (Fig. 13). The exhalation profile of ethane mirrors that of CO_2 and has a similar dead space, suggesting exhaled ethane arises from the alveolar region of the lungs. While both gases are normally assessed simultaneously, ethane appears to be more easily characterized analytically.

As analytical techniques have improved, the ability to reliably detect many compounds at much lower concentrations dramatically improved. A recent report detected and examined more than 100 VOCs presence in the exhaled breath, using gas chromatography at levels as low as 1 part per trillion (104). They correlated these compounds in the exhaled breath over time with blood glucose in diabetic children and identified a close correlation with methyl nitrate (CH_3NO_3). The mechanism underlying this correlation is not clear, but the CH_3NO_3 can be formed in an environment of high oxidative stress that includes superoxide and NO. Clearly, the potential use of CH_3NO_3 to noninvasively track blood glucose will need further investigation, but this initial report highlights the potential of exhaled breath biomarkers to track disease states.

Conclusion

All compounds that exist as gas at body temperature have the potential to exchange or interact with the airway tree. The extent of exchange, or rate of transfer, depends on several physical characteristics of both the gas and the airway tree including the solubility of the gas in water, the partial pressure difference between the airway wall and the airstream, chemical reaction that can produce or consume a gas, the airstream flow and pattern (i.e., laminar or turbulent), and the surface area of contact between the airway wall and airstream. The physical determinants of airway gas exchange can be influenced by the environment (e.g., high concentration of gas in the ambient air), age, gender, presence of disease, or physical activity. Prominent examples of gases with extensive exchange in the airways include NO and ethanol. Ethanol exchanges with the airways due to its high solubility in water, whereas NO is produced by cells present in the airways. A comprehensive understanding of airway gas exchange is necessary to interpret exhaled concentrations and thus identify gases that are useful breath biomarkers. While extensive research over the past decade has identified exhaled NO as a useful biomarker of airway inflammation, it is clear that hundreds of VOCs are present in the exhaled breath, providing rich opportunities for future investigation. The challenge is the reliable and reproducible detection of compounds at levels as low as 1 part per

trillion and then understanding the biochemical mechanisms that lead to their presence in the exhaled breath.

Acknowledgements

This work was supported, in part, by grants from the National Institutes of Health (R01 HL067954 and R01 HL070645).

References

1. Almstrand AC, Ljungstrom E, Lausmaa J, Bake B, Sjovall P, Olin AC. Airway monitoring by collection and mass spectrometric analysis of exhaled particles. *Anal Chem* 81: 662-668, 2009.
2. Alving K, Weitzberg E, Lundberg JM. Increased amount of nitric oxide in exhaled air of asthmatics. *Eur Respir J* 6: 1368-1370, 1993.
3. Anderson JC, Babb AL, Hlastala MP. Modeling soluble gas exchange in the airways and alveoli. *Ann Biomed Eng* 31: 1402-1422, 2003.
4. Anderson JC, Hlastala MP. Breath tests and airway gas exchange. *Pulm Pharmacol Ther* 20: 112-117, 2007.
5. Anderson JC, Hlastala MP. Impact of airway gas exchange on the multiple inert gas elimination technique. *Ann Biomed Eng* 38 (3): 1017-1030, 2010.
6. Anderson JC, Lamm WJ, Hlastala MP. Measuring airway exchange of endogenous acetone using a single-exhalation breathing maneuver. *J Appl Physiol* 100: 880-889, 2006.
7. Artlich A, Hagenah JU, Jonas S, Ahrens P, Gortner L. Exhaled nitric oxide in childhood asthma. *Eur J Pediatr* 155: 698-701, 1996.
8. Asplund PT, Ben-Jebria A, Rigas ML, Ultman JS. Longitudinal distribution of ozone absorption in the lung: Effect of continuous inhalation exposure. *Arch Environ Health* 51: 431-438, 1996.
9. Aulik IV. [Gas chromatographic analysis of exhaled air and acetylene mixture]. *Biull Eksp Biol Med* 62: 115-117, 1966.
10. Baker LG, Ultman JS, Rhoades RA. Simultaneous gas flow and diffusion in a symmetric airway system: A mathematical model. *Respir Physiol* 21: 119-138, 1974.
11. Baraldi E, Carraro S, Alinovi R, Pesci A, Ghiro L, Bodini A, Piacentini G, Zacchello F, Zanconato S. Cysteinyl leukotrienes and 8-isoprostane in exhaled breath condensate of children with asthma exacerbations. *Thorax* 58: 505-509, 2003.
12. Barreto M, Villa MP, Monti F, Bohmerova Z, Martella S, Montesano M, Darder MT, Ronchetti R. Additive effect of eosinophilia and atopy on exhaled nitric oxide levels in children with or without a history of respiratory symptoms. *Pediatr Allergy Immunol* 16: 52-58, 2005.
13. Bassett D, Elbon-Copp C, Otterbein S, Barraclough-Mitchell H, Delorme M, Yang H. Inflammatory cell availability affects ozone-induced lung damage. *J Toxicol Environ Health A* 64: 547-565, 2001.
14. Bates ML, Brenza TM, Ben-Jebria A, Bascom R, Ultman JS. Longitudinal distribution of ozone absorption in the lung: Comparison of cigarette smokers and nonsmokers. *Toxicol Appl Pharmacol* 236: 270-275, 2009.
15. Berkman N, Avital A, Breuer R, Bardach E, Springer C, Godfrey S. Exhaled nitric oxide in the diagnosis of asthma: Comparison with bronchial provocation tests. *Thorax* 60: 383-388, 2005.
16. Berry MA, Shaw DE, Green RH, Brightling CE, Wardlaw AJ, Pavord ID. The use of exhaled nitric oxide concentration to identify eosinophilic airway inflammation: An observational study in adults with asthma. *Clin Exp Allergy* 35: 1175-1179, 2005.
17. Bevan S, Geppetti P. Protons: Small stimulants of capsaicin-sensitive sensory nerves. *Trends Neurosci* 17: 509-512, 1994.
18. Bird RB, Stewart WE, Lightfoot EN. *Transport Phenomena*. New York: John Wiley & Sons, 1960.
19. Bissonnette EY, Hogaboam CM, Wallace JL, Befus AD. Potentiation of tumor necrosis factor-α-mediated cytotoxicity of mast cells by their production of nitric oxide. *J Immunol* 147: 3060-3065, 1991.
20. Borland C, Cox Y, Higenbottam T. Measurement of exhaled nitric oxide in man. *Thorax* 48: 1160-1162, 1993.
21. Bouhuys A. Respiratory dead space. In: *The Respiratory System. Gas Exchange*. Bethesda, MD, 1964, p. 699-714.
22. Brussee JE, Smit HA, Kerkhof M, Koopman LP, Wijga AH, Postma DS, Gerritsen J, Grobbee DE, Brunekreef B, de Jongste JC. Exhaled nitric oxide in four-year-old children: Relationship with asthma and atopy. *Eur Respir J* 25: 455-461, 2005.
23. Buchvald F, Baraldi E, Carraro S, Gaston B, De Jongste J, Pijnenburg MW, Silkoff PE, Bisgaard H. Measurements of exhaled nitric oxide in healthy subjects age 4 to 17 years. *J Allergy Clin Immunol* 115: 1130-1136, 2005.
24. Bush ML, Raybold T, Abeles S, Hu SC, Ben-Jebria A, Ultman JS. Longitudinal distribution of ozone absorption in the lung: Simulation with a single-path model. *Toxicol Appl Pharmacol* 140: 219-226, 1996.
25. Bush ML, Zhang W, Ben-Jebria A, Ultman JS. Longitudinal distribution of ozone and chlorine in the human respiratory tract: Simulation of nasal and oral breathing with the single-path diffusion model. *Toxicol Appl Pharmacol* 173: 137-145, 2001.
26. Busse R, Mulsch A. Induction of nitric oxide synthases by cytokines in vascular smooth muscle cells. *FEBS Lett* 275: 87-90, 1990.
27. Carpagnano GE, Barnes PJ, Francis J, Wilson N, Bush A, Kharitonov SA. Breath condensate pH in children with cystic fibrosis and asthma: A new noninvasive marker of airway inflammation? *Chest* 125: 2005-2010, 2004.
28. Carraro S, Folesani G, Corradi M, Zanconato S, Gaston B, Baraldi E. Acid-base equilibrium in exhaled breath condensate of allergic asthmatic children. *Allergy* 60: 476-481, 2005.
29. Condorelli P, George SC. Theoretical gas phase mass transfer coefficients for endogenous gases in the lung. *Ann Biomed Eng* 27 (3): 326-339, 1999.
30. Condorelli P, Shin HW, Aledia AS, Silkoff PE, George SC. A simple technique to characterize proximal and peripheral nitric oxide exchange using constant flow exhalations and an axial diffusion model. *J Appl Physiol* 102: 417-425, 2007.
31. Cope KA, Solga SF, Hummers LK, Wigley FM, Diehl AM, Risby TH. Abnormal exhaled ethane concentrations in scleroderma. *Biomarkers* 11: 70-84, 2006.
32. Cramer I. Heat and moisture exchange of respiratory mucous membranes. *Ann Otolo Rhinol Laryngol* 66: 327-343, 1957.
33. Dal Negro R, Micheletto C, Tognella S, Turco P, Rossetti A, Cantini L. Assessment of inhaled BDP-dose dependency of exhaled nitric oxide and local and serum eosinophilic markers in steroids-naive nonatopic asthmatics. *Allergy* 58: 1018-1022, 2003.
34. Davidson MR, Schroter RC. A theoretical model of absorption of gases by the bronchial wall. *J Fluid Mech* 129: 313-335, 1983.
35. De Gouw HW, Marshall-Partridge SJ, Van Der Veen H, Van Den Aardweg JG, Hiemstra PS, Sterk PJ. Role of nitric oxide in the airway response to exercise in healthy and asthmatic subjects. *J Appl Physiol* 90: 586-592, 2001.
36. Dragon CA, Grotberg JB. Oscillatory flow and dispersion in a flexible tube. *J Fluid Mech* 231: 135-155, 1991.
37. Dubois AB, Douglas JS, Stitt JT, Mohsenin V. Production and absorption of nitric oxide gas in the nose. *J Appl Physiol* 84: 1217-1224, 1998.
38. Dubois AB, Kelley PM, Douglas JS, Mohsenin V. Nitric oxide production and absorption in trachea, bronchi, bronchioles, and respiratory bronchioles of humans. *J Appl Physiol* 86: 159-167, 1999.
39. Dupont LJ, Demedts MG, Verleden GM. Prospective evaluation of the validity of exhaled nitric oxide for the diagnosis of asthma. *Chest* 123: 751-756, 2003.
40. Eckmann DM, Grotberg JB. Oscillatory flow and mass transport in a curved tube. *J Fluid Mech* 188: 509-527, 1988.
41. Elad D, Halpern D, Grotberg JB. Gas dispersion in volume-cycled tube flow. I. Theory. *J Appl Physiol* 72: 312-320, 1992.
42. Fang K, Johns R, Macdonald T, Kinter M, Gaston B. *S*-Nitrosoglutathione breakdown prevents airway smooth muscle relaxation in the guinea pig. *Am J Physiol Lung Cell Mol Physiol* 279: L716-L721, 2000.
43. Gage JC, Lagesson V, Tunek A. A method for the determination of low concentrations of organic vapours in air and exhaled breath. *Ann Occup Hyg* 20: 127-134, 1977.
44. Galassetti PR, Novak B, Nemet D, Rose-Gottron C, Cooper DM, Meinardi S, Newcomb R, Zaldivar F, Blake DR. Breath ethanol and acetone as indicators of serum glucose levels: An initial report. *Diabetes Technol Ther* 7: 115-123, 2005.
45. Garnier P, Fajac I, Dessanges JF, Dall'Ava-Santucci J, Lockhart A, Dinh-Xuan AT. Exhaled nitric oxide during acute changes of airways calibre in asthma. *Eur Respir J* 9: 1134-1138, 1996.
46. Gaston B, Drazen JM, Loscalzo J, Stamler JS. The biology of nitrogen oxides in the airways. *Am J Respir Crit Care Med* 149: 538-551, 1994.
47. Gaver DP III, Solway J, Punjabi N, Elad D, Grotberg JB, Gavriely N. Gas dispersion in volume-cycled tube flow. II. Tracer bolus experiments. *J Appl Physiol* 72: 321-331, 1992.
48. George SC, Babb AL, Hlastala MP. Dynamics of soluble gas exchange in the airways: III. Single exhalation breathing maneuver. *J Appl Physiol* 75: 2439-2449, 1993.
49. George SC, Babb AL, Hlastala MP. Modeling the concentration of ethanol in the exhaled breath following pre-test breathing maneuvers. *Ann Biomed Eng* 23: 48-60, 1995.
50. George SC, Hogman M, Permutt S, Silkoff PE. Modeling pulmonary nitric oxide exchange. *J Appl Physiol* 96: 831-839, 2004.

51. Grotberg J, Sheth BV, Mockros LF. An analysis of pollutant gas transport and absorption in pulmonary airways. *J Biomech Eng* 112: 168-176, 1990.
52. Grotberg JB. Gas absorption in pulmonary airways at low Peclet number. *J Biomech Eng* 112: 177-182, 1990.
53. Gustafsson LE, Leone AM, Persson MG, Wiklund NP, Moncada S. Endogenous nitric oxide is present in the exhaled air of rabbits, guinea pigs and humans. *Biochem Biophys Res Commun* 181: 852-857, 1991.
54. Hanna LM, Scherer PW. Measurement of local mass transfer coefficients in a cast model of the human upper respiratory tract. *J Biomech Eng* 108: 12-18, 1986.
55. Hanna LM, Scherer PW. A theoretical model of localized heat and water vapor transport in the human respiratory tract. *J Biomech Eng* 108: 19-27, 1986.
56. Hogman M, Drca N, Ehrstedt C, Merilainen P. Exhaled nitric oxide partitioned into alveolar, lower airways and nasal contributions. *Respir Med* 94: 985-991, 2000.
57. Holma B, Hegg PO. pH- and protein-dependent buffer capacity and viscosity of respiratory mucus. Their interrelationships and influence on health. *Sci Total Environ* 84: 71-82, 1989.
58. Hu SC, Ben-Jebria A, Ultman JS. Longitudinal distribution of ozone absorption in the lung: Quiet respiration in healthy subjects. *J Appl Physiol* 73: 1655-1661, 1992.
59. Hu S-C, Ben-Jebria A, Ultman JS. Longitudinal distribution of ozone absorption in the lung: Effects of respiratory flow. *J Appl Physiol* 77: 574-583, 1994.
60. Hunt JF, Fang K, Malik R, Snyder A, Malhotra N, Platts-Mills TA, Gaston B. Endogenous airway acidification. Implications for asthma pathophysiology. *Am J Respir Crit Care Med* 161: 694-699, 2000.
61. Ignarro LJ, Byrns RE, Buga GM, Wood KS. Endothelium-derived relaxing factor from pulmonary artery and vein possesses pharmacologic and chemical properties identical to those of nitric oxide radical. *Circ Res* 61: 866-879, 1987.
62. Inglestedt S. Studies on the conditioning of air in the respiratory tract. *Acta Otolaryngol Suppl* 131: 1-80, 1956.
63. Jiang J, Malavia N, Suresh V, George SC. Nitric oxide gas phase release in human small airway epithelial cells. *Respir Res* 10: 3, 2009.
64. Jones AW. Effects of temperature and humidity of inhaled air on the concentration of ethanol in a man's exhaled breath. *Clin Sci* 63: 441-445, 1982.
65. Jones AW. Determination of liquid/air partition coefficients for dilute solutions of ethanol in water, whole blood, and plasma. *J Anal Toxicol* 7: 193-197, 1983.
66. Jorens PG, VanOverveld FJ, Bult H, Vermiere PA, Herman AG. L-Arginine -dependent production of nitrogen oxides by rat pulmonary macrophages. *Eur J Pharmacol* 200: 205-209, 1991.
67. Jorens PG, VanOverveld FJ, Bult H, Vermeire PA, Herman AG. Synergism between interleukin-1 beta and interferon-gamma, an inducer of nitric oxide synthase, in rat lung fibroblasts. *Eur J Pharmacol* 224: 7-12, 1992.
68. Jorres RA. Modelling the production of nitric oxide within the human airways. *Eur Respir J* 16: 555-560, 2000.
69. Kabilan S, Lin CL, Hoffman EA. Characteristics of airflow in a CT-based ovine lung: A numerical study. *J Appl Physiol* 102: 1469-1482, 2007.
70. Kalapos MP. On the mammalian acetone metabolism: From chemistry to clinical implications. *Biochim Biophys Acta* 1621: 122-139, 2003.
71. Kanoh S, Kobayashi H, Motoyoshi K. Exhaled ethane: An *in vivo* biomarker of lipid peroxidation in interstitial lung diseases. *Chest* 128: 2387-2392, 2005.
72. Kazui M, Andreoni KA, Norris EJ, Klein AS, Burdick JF, Beattie C, Sehnert SS, Bell WR, Bulkley GB, Risby TH. Breath ethane: A specific indicator of free-radical-mediated lipid peroxidation following reperfusion of the ischemic liver. *Free Radic Biol Med* 13: 509-515, 1992.
73. Kerckx Y, Michils A, Van Muylem A. Airway contribution to alveolar nitric oxide in healthy subjects and stable asthma patients. *J Appl Physiol* 104: 918-924, 2008.
74. Kerr AA. Dead space ventilation in normal children and children with obstructive airways disease. *Thorax* 31: 63-69, 1976.
75. Kharitonov SA, Barnes PJ. Nasal contribution to exhaled nitric oxide during exhalation against resistance or during breath holding. *Thorax* 52: 540-544, 1997.
76. Kharitonov SA, Chung KF, Evans D, O'Connor BJ, Barnes PJ. Increased exhaled nitric oxide in asthma is mainly derived from the lower respiratory tract. *Am J Respir Crit Care Med* 153: 1773-1780, 1996.
77. Kharitonov SA, O'Connor BJ, Evans DJ, Barnes PJ. Allergen-induced late asthmatic reactions are associated with elevation of exhaled nitric oxide. *Am J Respir Crit Care Med* 151: 1894-1899, 1995.
78. Kharitonov SA, Yates D, Robbins RA, Logan-Sinclair R, Shinebourne EA, Barnes PJ. Increased nitric oxide in exhaled air of asthmatic patients. *Lancet* 343: 133-135, 1994.
79. Kimberly B, Nejadnik B, Giraud GD, Holden WE. Nasal contribution to exhaled nitric oxide at rest and during breathholding in humans. *Am J Respir Crit Care Med* 153: 829-836, 1996.
80. Kleinstreuer C, Zhang Z, Donohue JF. Targeted drug-aerosol delivery in the human respiratory system. *Annu Rev Biomed Eng* 10: 195-220, 2008.
81. Kleinstreuer C, Zhang Z, Li Z. Modeling airflow and particle transport/deposition in pulmonary airways. *Respir Physiol Neurobiol* 163: 128-138, 2008.
82. Kobzik L, Bredt D, Lowenstein C, Snyder SH, Drazen JM, Sugarbaker D, Stamler JS. Nitric oxide synthase in human and rat lung. *Am J Respir Cell Mol Biol* 9: 371-377, 1993.
83. Kostikas K, Papatheodorou G, Ganas K, Psathakis K, Panagou P, Loukides S. pH in expired breath condensate of patients with inflammatory airway diseases. *Am J Respir Crit Care Med* 165: 1364-1370, 2002.
84. Kotaru C, Coreno A, Skowronski M, Ciufo R, McFadden ER Jr. Exhaled nitric oxide and thermally induced asthma. *Am J Respir Crit Care Med* 163: 383-388, 2001.
85. Krishna MT, Blomberg A, Biscione GL, Kelly F, Sandstrom T, Frew A, Holgate S. Short-term ozone exposure upregulates P-selectin in normal human airways. *Am J Respir Crit Care Med* 155: 1798-1803, 1997.
86. Kupari M, Lommi J, Ventila M, Karjalainen U. Breath acetone in congestive heart failure. *Am J Cardiol* 76: 1076-1078, 1995.
87. Leuppi JD, Salome CM, Jenkins CR, Anderson SD, Xuan W, Marks GB, Koskela H, Brannan JD, Freed R, Andersson M, Chan HK, Woolcock AJ. Predictive markers of asthma exacerbation during stepwise dose reduction of inhaled corticosteroids. *Am J Respir Crit Care Med* 163: 406-412, 2001.
88. Lewis SM. Emptying patterns of the lung studied by multiple-breath N_2 washout. *J Appl Physiol* 44: 424-430., 1978.
89. Lex C, Payne DN, Zacharasiewicz A, Li AM, Wilson NM, Hansel TT, Bush A. Sputum induction in children with difficult asthma: Safety, feasibility, and inflammatory cell pattern. *Pediatr Pulmonol* 39: 318-324, 2005.
90. Lim S, Jatakanon A, Meah S, Oates T, Chung KF, Barnes PJ. Relationship between exhaled nitric oxide and mucosal eosinophilic inflammation in mild to moderately severe asthma. *Thorax* 55: 184-188, 2000.
91. Lim S, Tomita K, Caramori G, Jatakanon A, Oliver B, Keller A, Adcock I, Chung KF, Barnes PJ. Low-dose theophylline reduces eosinophilic inflammation but not exhaled nitric oxide in mild asthma. *Am J Respir Crit Care Med* 164: 273-276, 2001.
92. Little SA, Chalmers GW, MacLeod KJ, McSharry C, Thomson NC. Non-invasive markers of airway inflammation as predictors of oral steroid responsiveness in asthma. *Thorax* 55: 232-234, 2000.
93. Liu L, Hausladen A, Zeng M, Que L, Heitman J, Stamler JS. A metabolic enzyme for *S*-nitrosothiol conserved from bacteria to humans. *Nature* 410: 490-494, 2001.
94. Luchtel DL. The mucous layer of the trachea and major bronchi in the rat. *Scan Electron Microsc* 2: 1089-1098, 1978.
95. Luk CK, Dulfano MJ. Effect of pH, viscosity and ionic-strength changes on ciliary beating frequency of human bronchial explants. *Clin Sci (Lond)* 64: 449-451, 1983.
96. Lundberg JO, Farkas-Szallasi T, Weitzberg E, Rinder J, Lidholm J, Anggaard A, Hokfelt T, Lundberg JM, Alving K. High nitric oxide production in human paranasal sinuses. *Nat Med* 1: 370-373, 1995.
97. Malmberg LP, Turpeinen H, Rytila P, Sarna S, Haahtela T. Determinants of increased exhaled nitric oxide in patients with suspected asthma. *Allergy* 60: 464-468, 2005.
98. Miller FJ, Overton JH, Jaskot RH, Menzel DB. A model of the regional uptake of gaseous pollutants in the lung. *Toxicol Appl Pharmacol* 79: 11-27, 1985.
99. Montuschi P, Kharitonov SA, Ciabattoni G, Corradi M, van Rensen L, Geddes DM, Hodson ME, Barnes PJ. Exhaled 8-isoprostane as a new non-invasive biomarker of oxidative stress in cystic fibrosis. *Thorax* 55: 205-209, 2000.
100. Mork AK, Johanson G. A human physiological model describing acetone kinetics in blood and breath during various levels of physical exercise. *Toxicol Lett* 164: 6-15, 2006.
101. Nelson N, Lagesson V, Nosratabadi AR, Ludvigsson J, Tagesson C. Exhaled isoprene and acetone in newborn infants and in children with diabetes mellitus. *Pediatr Res* 44: 363-367, 1998.
102. Newport S, Amin N, Dozor AJ. Exhaled breath condensate pH and ammonia in cystic fibrosis and response to treatment of acute pulmonary exacerbations. *Pediatr Pulmonol* 44: 866-872, 2009.
103. Nodelman V, Ultman JS. Longitudinal distribution of chlorine absorption in human airways: A comparison to ozone absorption. *J Appl Physiol* 87: 2073-2080, 1999.
104. Novak BJ, Blake DR, Meinardi S, Rowland FS, Pontello A, Cooper DM, Galassetti PR. Exhaled methyl nitrate as a noninvasive marker of hyperglycemia in type 1 diabetes. *Proc Natl Acad Sci U S A* 104: 15613-15618, 2007.

105. Nowak N, Kakade PP, Annapragada AV. Computational fluid dynamics simulation of airflow and aerosol deposition in human lungs. *Ann Biomed Eng* 31: 374-390, 2003.
106. Obata H, Dittrick M, Chan H, Chan-Yeung M. Sputum eosinophils and exhaled nitric oxide during late asthmatic reaction in patients with western red cedar asthma. *Eur Respir J* 13: 489-495, 1999.
107. Ohlsson J, Ralph DD, Mandelkorn MA, Babb AL, Hlastala. MP. Accurate measurement of blood alcohol concentration with isothermal rebreathing. *J Stud Alcohol* 51: 6-13, 1990.
108. Olin AC, Aldenbratt A, Ekman A, Ljungkvist G, Jundgersten L, Alving K, Toren K. Increased nitric oxide in exhaled air after intake of a nitrate-rich meal. *Respir Med* 95: 153-158, 2001.
109. Onorato DJ, Demirozu MC, Breitenbucher A, Atkins ND, Chediak AD, Wanner A. Airway mucosal blood flow in humans. Response to adrenergic agonists. *Am J Respir Crit Care Med* 149: 1132-1137, 1994.
110. Paiva M, Engel LA. The anatomical basis for the sloping N_2 plateau. *Respir Physiol* 44: 325-337, 1981.
111. Paiva M, Engel LA. Theoretical studies of gas mixing and ventilation distribution in the lung. *Physiol Rev* 67: 750-796, 1987.
112. Pardaens J, Van de Woestijne KP, Clement J. A physical model of expiration. *J Appl Physiol* 33: 479-490, 1972.
113. Paredi P, Kharitonov SA, Barnes PJ. Elevation of exhaled ethane concentration in asthma. *Am J Respir Crit Care Med* 162: 1450-1454, 2000.
114. Paredi P, Kharitonov SA, Leak D, Ward S, Cramer D, Barnes PJ. Exhaled ethane, a marker of lipid peroxidation, is elevated in chronic obstructive pulmonary disease. *Am J Respir Crit Care Med* 162: 369-373, 2000.
115. Payne DN, Adcock IM, Wilson NM, Oates T, Scallan M, Bush A. Relationship between exhaled nitric oxide and mucosal eosinophilic inflammation in children with difficult asthma, after treatment with oral prednisolone. *Am J Respir Crit Care Med* 164: 1376-1381, 2001.
116. Peroni D, Bodini A, Miraglia Del Giudice M, Loiacono A, Baraldi E, Boner AL, Piacentini G. Effect of budesonide and montelukast in asthmatic children exposed to relevant allergens. *Allergy* 60: 206-210, 2005.
117. Perry RH, Green DW. *Perry's Chemical Engineers' Handbook*. New York: McGraw-Hill, 1984.
118. Persson MG, Wiklund NP, Gustafsson LE. Endogenous nitric oxide in single exhalations and the change during exercise. *Am Rev Respir Dis* 148: 1210-1214, 1993.
119. Pietropaoli AP, Perillo IB, Torres A, Perkins PT, Frasier LM, Utell MJ, Frampton MW, Hyde RW. Simultaneous measurement of nitric oxide production by conducting and alveolar airways of humans. *J Appl Physiol* 87: 1532-1542, 1999.
120. Pijnenburg MW, Hofhuis W, Hop WC, De Jongste JC. Exhaled nitric oxide predicts asthma relapse in children with clinical asthma remission. *Thorax* 60: 215-218, 2005.
121. Prisk GK, Elliott AR, Guy HJ, Verbanck S, Paiva M, West JB. Multiple-breath washin of helium and sulfur hexafluoride in sustained microgravity. *J Appl Physiol* 84: 244-252, 1998.
122. Prisk GK, Guy HJ, Elliott AR, Paiva M, West JB. Ventilatory inhomogeneity determined from multiple-breath washouts during sustained microgravity on Spacelab SLS-1. *J Appl Physiol* 78: 597-607, 1995.
123. Ratnawati, Morton J, Henry RL, Thomas PS. Exhaled breath condensate nitrite/nitrate and pH in relation to pediatric asthma control and exhaled nitric oxide. *Pediatr Pulmonol* 41: 929-936, 2006.
124. Reid RC, Frausnitz JM, Poling BE. *The Properties of Gases and Liquids*. New York: McGraw-Hill, 1988.
125. Ricciardolo FL, Geppetti P, Mistretta A, Nadel JA, Sapienza MA, Bellofiore S, Di Maria GU. Randomised double-blind placebo-controlled study of the effect of inhibition of nitric oxide synthesis in bradykinin-induced asthma. *Lancet* 348: 374-377, 1996.
126. Rigas ML, Ben-Jebria A, Ultman JS. Longitudinal distribution of ozone absorption in the lung: Effects of nitrogen dioxide, sulfur dioxide, and ozone exposures. *Arch Environ Health* 52: 173-178, 1997.
127. Rimele TJ, Sturm RJ, Adams LM, Henry DE, Heaslip RJ, Weichman BM, Grimes D. Interaction of neutrophils with smooth muscle: Identification of a neutrophil-derived relaxing factor. *J Pharmacol Exp Ther* 245: 102-111, 1988.
128. Sacco O, Sale R, Silvestri M, Serpero L, Sabatini F, Raynal ME, Biraghi M, Rossi GA. Total and allergen-specific IgE levels in serum reflect blood eosinophilia and fractional exhaled nitric oxide concentrations but not pulmonary functions in allergic asthmatic children sensitized to house dust mites. *Pediatr Allergy Immunol* 14: 475-481, 2003.
129. Sapienza MA, Kharitonov SA, Horvath I, Chung KF, Barnes PJ. Effect of inhaled L-arginine on exhaled nitric oxide in normal and asthmatic subjects. *Thorax* 53: 172-175, 1998.
130. Sartori C, Lepori M, Busch T, Duplain H, Hildebrandt W, Bartsch P, Nicod P, Falke KJ, Scherrer U. Exhaled nitric oxide does not provide a marker of vascular endothelial function in healthy humans. *Am J Respir Crit Care Med* 160: 879-882, 1999.
131. Scherer PW, Gobran S, Aukburg SJ, Baumgardner JE, Bartkowski R, Neufeld GR. Numerical and experimental study of steady-state CO_2 and inert gas washout. *J Appl Physiol* 64: 1022-1029, 1988.
132. Scherer PW, Shendalman LH, Greene NM, Bouhuys A. Measurement of axial diffusivities in a model of the bronchial airways. *J Appl Physiol* 38: 719-723, 1975.
133. Schroter RC, Sudlow MF. Flow patterns in models of the human bronchial airways. *Respir Physiol* 7: 341-355, 1969.
134. Schroter RC, Sudlow MF. Velocity profiles in models of human airways. *J Physiol* 202: 36P-37P, 1969.
135. Scuri M, McCaskill V, Chediak AD, Abraham WM, Wanner A. Measurement of airway mucosal blood flow with dimethylether: Validation with microspheres. *J Appl Physiol* 79: 1386-1390, 1995.
136. Shier D, Butler J, Lewis R. *Hole's Human Anatomy and Physiology*. Boston, MA: McGraw Hill, 1999.
137. Shin H-W, Condorelli P, George SC. Examining axial diffusion of nitric oxide in the lungs using heliox and breath hold. *J Appl Physiol* 100: 623-630, 2006.
138. Shin H-W, Condorelli P, Rose-Gottron CM, Cooper DM, George SC. Probing the impact of axial diffusion on nitric oxide exchange dynamics with heliox. *J Appl Physiol* 97: 874-882, 2004.
139. Shin H-W, George SC. Microscopic modeling of NO and *S*-nitrosoglutathione kinetics and transport in human airways. *J Appl Physiol* 90: 777-788, 2001.
140. Shin H-W, George SC. Impact of axial diffusion on nitric oxide exchange in the lungs. *J Appl Physiol* 93: 2070-2080, 2002.
141. Shin H-W, Rose-Gottron CM, Perez F, Cooper DM, Wilson AF, George SC. Flow-independent nitric oxide exchange parameters in healthy adults. *J Appl Physiol* 91: 2173-2181, 2001.
142. Silkoff PE, McClean PA, Caramori M, Slutsky AS, Zamel N. A significant proportion of exhaled nitric oxide arises in large airways in normal subjects. *Respir Physiol* 113: 33-38, 1998.
143. Silkoff PE, McClean PA, Slutsky AS, Furlott HG, Hoffstein E, Wakita S, Chapman KR, Szalai JP, Zamel N. Marked flow-dependence of exhaled nitric oxide using a new technique to exclude nasal nitric oxide. *Am J Respir Crit Care Med* 155: 260-267, 1997.
144. Silkoff PE, Sylvester JT, Zamel N, Permutt S. Airway nitric oxide diffusion in asthma. Role in pulmonary function and bronchial responsiveness. *Am J Respir Crit Care Med* 161: 1218-1228, 2000.
145. Silvestri M, Sabatini F, Sale R, Defilippi AC, Fregonese L, Battistini E, Biraghi MG, Rossi GA. Correlations between exhaled nitric oxide levels, blood eosinophilia, and airway obstruction reversibility in childhood asthma are detectable only in atopic individuals. *Pediatr Pulmonol* 35: 358-363, 2003.
146. Silvestri M, Sabatini F, Spallarossa D, Fregonese L, Battistini E, Biraghi MG, Rossi GA. Exhaled nitric oxide levels in non-allergic and allergic mono- or polysensitised children with asthma. *Thorax* 56: 857-862, 2001.
147. Silvestri M, Spallarossa D, Frangova Yourukova V, Battistini E, Fregonese B, Rossi GA. Orally exhaled nitric oxide levels are related to the degree of blood eosinophilia in atopic children with mild-intermittent asthma. *Eur Respir J* 13: 321-326, 1999.
148. Smith AD, Cowan JO, Brassett KP, Herbison GP, Taylor DR. Use of exhaled nitric oxide measurements to guide treatment in chronic asthma. *N Engl J Med* 352: 2163-2173, 2005.
149. Smith D, Spanel P, Davies S. Trace gases in breath of healthy volunteers when fasting and after a protein-calorie meal: A preliminary study. *J Appl Physiol* 87: 1584-1588, 1999.
150. Souders JE, George SC, Polissar NL, Swenson ER, Hlastala MP. Tracheal gas exchange: Perfusion-related differences in inert gas elimination. *J Appl Physiol* 79: 918-928, 1995.
151. Steerenberg PA, Janssen NA, de Meer G, Fischer PH, Nierkens S, van Loveren H, Opperhuizen A, Brunekreef B, van Amsterdam JG. Relationship between exhaled NO, respiratory symptoms, lung function, bronchial hyperresponsiveness, and blood eosinophilia in school children. *Thorax* 58: 242-245, 2003.
152. Suresh V, Mih JD, George SC. Measurement of IL-13-induced iNOS-derived gas phase nitric oxide in human bronchial epithelial cells. *Am J Respir Cell Mol Biol* 37: 97-104, 2007.
153. Suresh V, Shelley DA, Shin HW, George SC. Effect of heterogeneous ventilation and nitric oxide production on exhaled nitric oxide profiles. *J Appl Physiol* 104: 1743-1752, 2008.
154. Swenson ER, Robertson HT, Polissar NL, Middaugh ME, Hlastala MP. Conducting airway gas exchange: Diffusion related differences in inert gas elimination. *J Appl Physiol* 72: 1581-1588, 1992.
155. Szefler SJ, Martin RJ, King TS, Boushey HA, Cherniack RM, Chinchilli VM, Craig TJ, Dolovich M, Drazen JM, Fagan JK, Fahy JV, Fish JE, Ford JG, Israel E, Kiley J, Kraft M, Lazarus SC, Lemanske RF Jr, Mauger E, Peters SP, Sorkness CA. Significant variability in response to inhaled corticosteroids for persistent asthma. *J Allergy Clin Immunol* 109: 410-418, 2002.

156. ten Brinke A, Zwinderman AH, Sterk PJ, Rabe KF, Bel EH. Factors associated with persistent airflow limitation in severe asthma. *Am J Respir Crit Care Med* 164: 744-748, 2001.
157. Tsoukias NM, George SC. A two-compartment model of pulmonary nitric oxide exchange dynamics. *J Appl Physiol* 85: 653-666, 1998.
158. Tsoukias NM, Shin H-W, Wilson AF, George SC. A single breath technique with variable flow rate to characterize nitric oxide exchange dynamics in the lungs. *J Appl Physiol* 91: 477-487, 2001.
159. Tsoukias NM, Tannous Z, Wilson AF, George SC. Single-exhalation profiles of NO and CO_2 in humans: Effect of dynamically changing flow rate. *J Appl Physiol* 85: 642-652, 1998.
160. Tsu ME, Babb AL, Ralph DD, Hlastala MP. Dynamics of heat, water, and soluble gas exchange in the human airways: I. A model study. *Ann Biomed Eng* 16: 547-571, 1988.
161. Tsu ME, Babb AL, Sugiyama EM, Hlastala MP. Dynamics of soluble gas exchange in the airways: II. Effects of breathing conditions. *Respir Physiol* 83: 261-276, 1991.
162. Turner C, Spanel P, Smith D. A longitudinal study of ammonia, acetone and propanol in the exhaled breath of 30 subjects using selected ion flow tube mass spectrometry, SIFT-MS. *Physiol Meas* 27: 321-337, 2006.
163. Ultman JS, Blatman HS. Longitudinal mixing in pulmonary airways: Analysis of inert gas dispersion i symmetric tube network models. *Respir Physiol* 30: 349-367, 1977.
164. Uysal N, Schapira RM. Effects of ozone on lung function and lung diseases. *Curr Opin Pulm Med* 9: 144-150, 2003.
165. Van Muylem A, Noel C, Paiva M. Modeling of impact of gas molecular diffusion on nitric oxide expired profile. *J Appl Physiol* 94: 119-127, 2003.
166. Verbanck S, Paiva M. Model simulations of gas mixing and ventilation distribution in the human lung. *J Appl Physiol* 69: 2269-2279, 1990.
167. von Basum G, Dahnke H, Halmer D, Hering P, Murtz M. Online recording of ethane traces in human breath via infrared laser spectroscopy. *J Appl Physiol* 95: 2583-2590, 2003.
168. Wanner A, Mendes ES, Atkins ND. A simplified noninvasive method to measure airway blood flow in humans. *J Appl Physiol* 100: 1674-1678, 2006.
169. Weibel E. *Morphometry of the Human Lung*. Berlin: Springler-Verlag, 1963.
170. Wood LD, Prichard S, Weng TR, Kruger K, Bryan AC, Levison H. Relationship between anatomic dead space and body size in health, asthma, and cystic fibrosis. *Am Rev Respir Dis* 104: 215-222., 1971.
171. Wyse C, Cathcart A, Sutherland R, Ward S, McMillan L, Gibson G, Padgett M, Skeldon K. Effect of maximal dynamic exercise on exhaled ethane and carbon monoxide levels in human, equine, and canine athletes. *Comp Biochem Physiol A Mol Integr Physiol* 141: 239-246, 2005.
172. Yates DH, Kharitonov SA, Robbins RA, Thomas PS, Barnes PJ. Effect of a nitric oxide synthase inhibitor and a glucocorticosteroid on exhaled nitric oxide. *Am J Respir Crit Care Med* 152: 892-896, 1995.
173. Yates DH, Kharitonov SA, Thomas PS, Barnes PJ. Endogenous nitric oxide is decreased in asthmatic patients by an inhibitor of inducible nitric oxide synthase. *Am J Respir Crit Care Med* 154: 247-250, 1996.
174. Yeates DB, Aspin N. A mathematical description of the airways of the human lungs. *Respir Physiol* 32: 91-104, 1978.
175. Yu CP. On equation of gas transport in the lung. *Respir Physiol* 23: 257-266, 1975.